

# Type-Based Unsourced Multiple Access Over Fading Channels in Distributed MIMO With Application to Multi-Target Localization

Kaan Okumus, *Graduate Student Member, IEEE*, Khac-Hoang Ngo, *Member, IEEE*, Giuseppe Durisi, *Senior Member, IEEE*, Erik G. Ström, *Fellow, IEEE*

**Abstract**—We consider the problem of type estimation over unsourced multiple access fading channels in distributed multiple-input multiple-output (D-MIMO) systems. Unlike classical unsourced multiple access, type-based unsourced multiple access (TUMA) aims to estimate the type, i.e., the empirical distribution of transmitted messages. We extend our prior work on TUMA over additive white Gaussian channels to fading scenarios in which neither the transmitters nor the receiver have channel state information. To mitigate the impact of path-loss variability, we employ location-based codebook partitioning: users with similar large-scale fading coefficients use the same codebook. The decoder is built on the multisource approximate message passing algorithm proposed by Çakmak *et al.* (2025), and supports both centralized and distributed implementations. As an application, we demonstrate how TUMA enables efficient communication in a multi-target localization setting, where distributed sensors report to a D-MIMO receiver quantized target positions. We propose a performance cost function that combines localization errors with a misdetection penalty, and use it to characterize how performance depends on the fraction of resources assigned to sensing vs. communication, as well as on the number of bits used to quantize the positions of the targets.

**Index Terms**—Type-based unsourced multiple access, massive random access, distributed MIMO, approximate message passing, multi-target localization.

## I. INTRODUCTION

MASSIVE machine-type communication (mMTC) is a key enabler for emerging 6G applications: it supports simultaneous transmissions from a large number of devices over a shared wireless medium. These devices typically transmit short packets in a sporadic and uncoordinated manner and operate under strict energy constraints [3]–[5]. With the need to support massive device connectivity, any scheme that assigns dedicated resources such as time, frequency, or codes to each device is not scalable. To address this challenge,

Kaan Okumus, Giuseppe Durisi, and Erik G. Ström are with the Department of Electrical Engineering, Chalmers University of Technology, 41296 Gothenburg, Sweden (email: {okumus, durisi, erik.strom}@chalmers.se).

Khac-Hoang Ngo is with the Department of Electrical Engineering, Linköping University, 58183 Linköping, Sweden (email: khac-hoang.ngo@liu.se).

This work was supported in part by the Swedish Research Council under grants 2021-04970 and 2022-04471, and by the Swedish Foundation for Strategic Research. The work of K.-H. Ngo was supported in part by the Excellence Center at Linköping – Lund in Information Technology (ELLIIT). This paper was presented in part at the IEEE International Workshop on Signal Processing Advances in Wireless Communications (SPAWC), Lucca, Italy, 2024 [1] and at the IEEE International Symposium on Information Theory (ISIT), Ann Arbor, Michigan, USA, 2025 [2].

the unsourced multiple access (UMA) framework was introduced [6]. In UMA, all users share a common codebook and the receiver is tasked with recovering the list of transmitted messages without identifying their sources. Recent significant theoretical and algorithmic advances in this area include the analysis of fundamental limits [7]–[11] on progressively more realistic channel models, and the design of coding schemes approaching these limits [11]–[19]. A key assumption in UMA is that the event where multiple devices transmit the same message simultaneously, known as message collision, is treated as a decoding error. This is justified because, when each device selects its message independently and uniformly at random from a large message set, the probability of message collisions is negligible. However, this assumption is often violated in practical sensing and learning applications, where multiple users may observe the same phenomenon and generate identical messages. Examples include multi-target localization [20]–[22], where sensors may report the same target position; federated learning [23], [24], where clients may transmit the same quantized model updates due to similarities in their local data; and point-cloud transmission [25], where devices observing the same surface may produce identical descriptors. In such cases, message collisions occur naturally and can no longer be neglected. On the contrary, it is critical that the decoder provides an estimate of the multiplicity of each message. This motivates the need for a generalized UMA framework, in which the multiplicity of each message is reliably estimated. This paper addresses this gap by proposing type-based UMA (TUMA), which handles the estimation of message multiplicities over fading channels in a distributed multiple-input multiple-output (D-MIMO) architecture.

### A. Related Works

Estimating the multiplicity of each message is equivalent to characterizing the empirical distribution (also known as “type”) of the messages. An early formulation of type-based estimation appeared in the context of distributed detection in wireless sensor networks [26], where sensors transmit local type summaries to a fusion center. This idea was later formalized under the name of type-based multiple access in [27], where message multiplicities are estimated via the use of orthogonal codebooks. This approach, however, suffers from limited scalability, due to the high spectral efficiency cost of orthogonality. To overcome this limitation, recent

works extended type-based multiple access to nonorthogonal codebooks [28]–[30]. However, these works consider only a small message set and do not address the massive and sporadic device activity that is typical in massive random access. A type estimation scheme with nonorthogonal codebooks has also been presented in [23] in the context of over-the-air computation for federated learning, but the proposed approximate message passing (AMP)-based digital aggregation (AMP-DA) decoder requires perfect channel state information (CSI) at the transmitter side to perform channel pre-equalization. A general type-based access framework supporting nonorthogonal transmissions, a large message space and a massive number of sporadically activated devices, and operating under practical constraints, such as the lack of CSI, is not available in the literature.

To address these limitations, in our previous work [1], we introduced the TUMA framework—a general communication-theoretic solution for estimating message types under collisions. TUMA supports massive uncoordinated access with nonorthogonal codewords and enables type estimation via Bayesian inference. In [1], three decoder architectures were considered: two based on expectation propagation techniques adopted from [31], and one based on the AMP decoder from [12]. We showed that the AMP-based decoder achieves superior performance in terms of complexity and estimation accuracy. In [32], we also derived an achievability bound for TUMA and showed a good agreement between the bound and the performance achievable using a practical coded compressed sensing (CCS)-AMP scheme [33], adapted for TUMA. The analysis in [1], [32] is, however, conducted for a simplified Gaussian channel model, in which small-scale fading is absent and all users are received at the same power.

Such limitations have recently been overcome in [34]–[36], where the authors analyze UMA over D-MIMO network architectures. The analysis in [34]–[36] relies on two key ideas: i) the assumption that an accurate model for the large-scale fading coefficients (LSFCs) at each point in the coverage area is available at the receiver; ii) the use of location-based codebook partitioning, where each user selects its codebook based on its LSFC profile. For this setup, in [34]–[36], a decoding algorithm, referred to as multisource AMP, is proposed, which allows for the estimation of the transmitted messages, the channel statistics, and the user location without requiring any knowledge of the instantaneous CSI. The use of a location-based codebook partitioning is advantageous, because it allows one to use a more concentrated prior for the path-loss vector at the denoiser, which is beneficial in terms of performance. However, the analysis in [34]–[36] does not address type estimation.

## B. Contributions

In this work, we extend the TUMA framework to support a more realistic system model and evaluate it in a multi-target localization application. Our contributions are as follows:

*TUMA over fading channels in D-MIMO with random user activity:* We generalize the TUMA framework in [2] by including both small- and large- scale fading and by assuming

that the number of active users is random and unknown to the receiver. As in [35], we assume perfect knowledge of LSFC at each point in the coverage area and employ location-based codebook partitioning. We adapt the multisource AMP algorithm proposed in [35] to TUMA by modifying the Bayesian denoiser to account for message multiplicities. In multisource AMP, the denoiser estimates, for each codeword, the combined fading coefficients of all users who transmitted that codeword. Under message collisions, this requires integrating over multiple unknown user positions, which leads to high complexity. We employ Monte Carlo (MC) sampling to approximate these integrals. We also modify the Onsager correction term, which compensates for correlation across AMP iterations, to ensure consistency with the modified denoiser. Based on the AMP outputs, we perform Bayesian estimation of the message multiplicities and normalize them to obtain the estimated type. We additionally introduce a distributed variant of our decoder, inspired by the distributed AMP (dAMP) algorithm [37], originally proposed in the context of activity detection under perfect per user LSFC information. The distributed variant leads to a lower computational complexity, which makes it suitable for large-scale D-MIMO systems.

*Application to multi-target localization and end-to-end tradeoff evaluation:* We demonstrate how TUMA can be applied to multi-target localization, where distributed sensors detect targets and transmit their quantized positions via un-sourced access. The sensing model used in our system is based on a practical millimeter-wave (mmWave) 5G simultaneous localization and mapping (SLAM) scenario, with detection probabilities depending on the path-loss [38]. For this setting, we introduce a prior on the message multiplicities that reflects the sensing model. To assess performance, we fix a total transmission blocklength and split it into a phase devoted to target sensing and one devoted to communication of the estimated target positions. A larger sensing blocklength improves detection but reduces the blocklength available for communication, which degrades type estimation. A large communication blocklength has the opposite effect. The quantization resolution adds a third component to this tradeoff: using more bits reduces localization error but enlarges the message space, making type estimation more challenging.

To evaluate these effects, we employ complementary metrics. We use total variation (TV) distance to measure communication errors, and Wasserstein distance to measure localization errors, reflecting both quantization and communication effects. We further use empirical misdetection probability to quantify sensing performance. We combine Wasserstein distance and empirical misdetection probability into a novel cost function, which is inspired by the generalized optimal sub-pattern assignment (GOSPA) metric [22]. We use the proposed GOSPA-like metric to investigate, via numerical simulations, how multi-target localization performance depends on the fraction of blocklength devoted to sensing vs. communication, as well as on the resolution of the quantizer used to describe the positions of the targets.

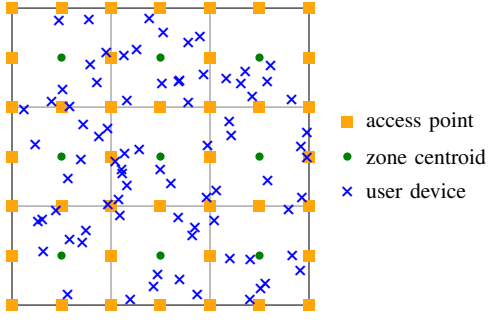


Fig. 1. An example of the proposed zone partitioning. In the example, we have  $U = 9$  zones. This partitioning is compatible with the distance-dependent path-loss model described in Section V-A.

### C. Paper Outline

The remainder of the paper is organized as follows. In Section II, we introduce the proposed TUMA framework, including the encoder, the channel model, and the type-based decoder. In Section III, we describe in detail the decoding algorithm, covering the multisource AMP formulation and the modified Bayesian denoiser. We also present an efficient MC approximation of the high-dimensional integrals appearing in the decoding algorithm and a distributed implementation. In Section IV, we discuss how to use TUMA in a multi-target localization scenario, introduce the sensing model and prior, and define the relevant performance metrics. In Section V, we provide simulation results, unveiling the tradeoff between sensing, quantization, and communication. We conclude the paper in Section VI.

### D. Notation

We denote system parameters by nonitalic uppercase letters (e.g.,  $A$ ), sets by calligraphic letters (e.g.,  $\mathcal{S}$ ), scalar variables by italic lowercase letters (e.g.,  $x$ ), vectors by boldface italic lowercase letters (e.g.,  $\mathbf{x}$ ), and matrices by boldface nonitalic uppercase letters (e.g.,  $\mathbf{X}$ ). We write the  $(a, b)$ th element of  $\mathbf{X}$  as  $[\mathbf{X}]_{a,b}$ , and the  $b$ th element of  $\mathbf{x}$  as  $[\mathbf{x}]_b$ . We denote the  $n \times n$  identity matrix by  $\mathbf{I}_n$ , and the all-zero vector by  $\mathbf{0}$ . Transposition and Hermitian transposition are indicated by the superscripts  $\text{T}$  and  $\text{H}$ , respectively. We denote the complex proper Gaussian vector distribution with mean  $\mathbf{0}$  and covariance  $\mathbf{A}$  by  $\mathcal{CN}(\mathbf{0}, \mathbf{A})$ , and its probability density function by  $\mathcal{CN}(\cdot; \mathbf{0}, \mathbf{A})$ . The Binomial distribution with  $n$  trials and success probability  $p$  is denoted by  $\text{Bin}(n, p)$ , and its probability mass function by  $\text{Bin}(\cdot; n, p)$ . The uniform distribution over the interval  $[a, b]$  is denoted by  $\text{Unif}(a, b)$  and the  $\ell_p$ -norm by  $\|\cdot\|_p$ ;  $[n]$  stands for  $\{1, \dots, n\}$ . We denote the Kronecker delta function by  $\delta(\cdot)$ , the indicator function by  $\mathbb{1}\{\cdot\}$ , the Kronecker product by  $\otimes$ , and elementwise multiplication by  $\odot$ ;  $\text{diag}(x_1, \dots, x_n)$  is a diagonal matrix with  $x_1, \dots, x_n$  as its diagonal entries. The notation  $\sim_{\text{i.i.d.}}$  indicates that the elements of a matrix are drawn independently from the specified distribution. Finally, we denote the probability simplex over the set  $[\mathbf{M}]$  by  $\mathcal{P}([\mathbf{M}])$ .

## II. SYSTEM MODEL

We consider a D-MIMO network in which  $B$  access points (APs) are connected to a central processing unit (CPU) via fronthaul links. The APs collaboratively serve single-antenna users, randomly located in a two-dimensional coverage area  $\mathcal{D}$ . The area is partitioned into  $U$  nonoverlapping zones  $\{\mathcal{D}_u\}_{u \in [U]}$ , such that  $\mathcal{D} = \bigcup_{u \in [U]} \mathcal{D}_u$  and  $\mathcal{D}_u \cap \mathcal{D}_{u'} = \emptyset, \forall u \neq u'$ . Each zone contains locations with similar LSFCs, so that users within the same zone experience approximately the same path-loss towards the APs. This partitioning mitigates the effect of path-loss variability [35].<sup>1</sup> Each AP  $b$  is located at position  $\nu_b \in \mathcal{D}$  and equipped with  $A$  antennas, yielding  $F = A \times B$  antennas in total. Fig. 1 illustrates an example of the network topology, where the area is divided into a  $3 \times 3$  grid of square zones, with APs evenly placed along the zone boundaries. While our model and design are applicable to general topologies as long as users with similar path-loss are grouped within the same zone, we use this specific topology in the simulations in Section V.

We assume that  $K$  users are present in the system, with  $K$  fixed and known by the receiver. In each communication round, a random subset of the users becomes active. The number of active users, denoted by  $K_a$ , is random and unknown to the receiver. Within each zone  $u$ , the number of active users, denoted by  $K_{a,u}$ , is also random and unknown, with  $K_a = \sum_{u=1}^U K_{a,u}$ . Each active user  $k$  in zone  $u$  selects a message  $W_{u,k}$  from the message set  $[\mathbf{M}]$ , where  $M$  is the total number of possible messages. These messages might be quantized representations of application-specific information, such as target positions in multi-target localization or local model updates in federated learning. In Section IV, we will focus on multi-target localization and provide a specific mechanism for user activation and message generation in such a setup.

The overall TUMA framework, including message encoding, transmission over the fading channel, and decoding at the receiver, is summarized in Fig. 2. Next, we provide a detailed description of each block in the figure.

### A. Encoder

The system employs a UMA codebook  $\mathbf{C} \in \mathbb{C}^{N_c \times \bar{M}}$ , where  $N_c$  is the blocklength and  $\bar{M} = U \cdot M$  is the total number of codewords. The codebook is evenly partitioned into zone-specific subcodebooks:  $\mathbf{C} = [\mathbf{C}_1, \dots, \mathbf{C}_U]$ , where  $\mathbf{C}_u = [\mathbf{c}_{u,1}, \dots, \mathbf{c}_{u,M}] \in \mathbb{C}^{N_c \times M}$ . The set of column vectors of  $\mathbf{C}_u$  forms the set of codewords for zone  $u$ , denoted as  $\mathcal{C}_u = \{\mathbf{c}_{u,1}, \dots, \mathbf{c}_{u,M}\}$ , where  $\|\mathbf{c}_{u,m}\|_2^2 = 1, \forall u \in [U], m \in [M]$ . The encoder  $\text{enc}_u : [\mathbf{M}] \rightarrow \mathcal{C}_u$  maps each message  $W_{u,k}$  to the codeword  $\text{enc}_u(W_{u,k}) = \mathbf{c}_{u,W_{u,k}}$ . Note that all users within the same zone use the same encoder.

### B. Multiplicity and Type

We denote the number of users transmitting message  $m$  in zone  $u$  by  $k_{u,m} \in \{0, 1, \dots, K_{a,u}\}$ . These form the multiplicity

<sup>1</sup>In practice, one can divide  $\mathcal{D}$  into  $U$  zones by quantizing the LSFC vector at each position in  $\mathcal{D}$  using a codebook of size  $U$ . Each client then estimates its LSFC coefficients using control signals transmitted by each AP, and selects its zone, and, hence, the corresponding codebook, on the basis of its quantized estimated LSFC vector.

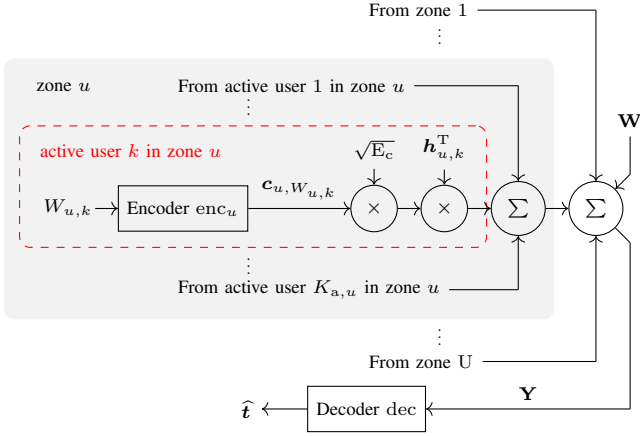


Fig. 2. Block diagram of the proposed TUMA framework with fading channel in a D-MIMO system.

ity vector  $\mathbf{k}_u = [k_{u,1}, \dots, k_{u,M}]^T$  with  $\|\mathbf{k}_u\|_1 = K_{a,u}$ . The global multiplicity vector is defined as  $\mathbf{k} = [k_1, \dots, k_M]^T$  with  $k_m = \sum_{u=1}^U k_{u,m}$ . The type is then obtained as the vector of normalized multiplicities, i.e.,  $\mathbf{t} = [t_1, \dots, t_M]^T$  with  $t_m = k_m/K_a$ . This vector represents the empirical distribution of transmitted messages across all active users.

### C. Channel Model

We index by  $(u, k)$  the  $k$ th active user in zone  $u$ . The channel between active user  $(u, k)$  and AP  $b$  is modeled as a quasi-static Rayleigh fading channel. Specifically, the channel coefficients are assumed to be independent across antennas, APs, and users, and to stay constant over the duration of a codeword. The channel vector  $\mathbf{h}_{u,k} \in \mathbb{C}^F$  between active user  $(u, k)$  and all receive antennas is distributed as  $\mathcal{CN}(\mathbf{0}, \Sigma(\boldsymbol{\rho}_{u,k}))$ , where  $\boldsymbol{\rho}_{u,k}$  denotes the position of active user  $(u, k)$  and  $\Sigma(\boldsymbol{\rho}_{u,k}) = \text{diag}(\gamma_1(\boldsymbol{\rho}_{u,k}), \dots, \gamma_B(\boldsymbol{\rho}_{u,k})) \otimes \mathbf{I}_A$  with  $\gamma_b(\boldsymbol{\rho}_{u,k})$  being the position-specific LSFC. When multiple users transmit the same codeword, their contributions are superimposed at the receiver. For a codeword  $\mathbf{c}_{u,m}$ , the effective channel vector is given by

$$\mathbf{x}_{u,m} = \begin{cases} \sum_{k \in [K_{a,u}] : W_{u,k} = m} \mathbf{h}_{u,k} & \text{if } k_{u,m} > 0, \\ \mathbf{0} & \text{if } k_{u,m} = 0. \end{cases} \quad (1)$$

Collecting the effective channel vectors for all codewords in zone  $u$ , we define the effective channel matrix as  $\mathbf{X}_u = [\mathbf{x}_{u,1}, \dots, \mathbf{x}_{u,M}]^T \in \mathbb{C}^{M \times F}$ . The aggregated received signal across all APs is then given by

$$\mathbf{Y} = \sqrt{E_c} \sum_{u=1}^U \mathbf{C}_u \mathbf{X}_u + \mathbf{W} \in \mathbb{C}^{N_c \times F}, \quad (2)$$

where  $\mathbf{W} \sim_{\text{i.i.d.}} \mathcal{CN}(0, \sigma_w^2)$  is the AWGN. The per-codeword average transmit energy is denoted by  $E_c$ , and the transmit signal to noise ratio (SNR) is defined as  $\text{SNR}_{\text{tx}} = E_c / (N_c \sigma_w^2)$ .

### D. Decoder

The decoder estimates the message type by using a decoding function defined as  $\text{dec} : \mathbb{C}^{N_c \times F} \rightarrow \mathcal{P}([M])$ . Given  $\mathbf{Y}$

and  $\mathbf{C}$ , the decoder first estimates the per-zone multiplicities,  $\hat{\mathbf{k}}_u = [k_{u,1}, \dots, k_{u,M}]^T$ ,  $u = 1, \dots, U$ , and then computes the global multiplicity vector,  $\hat{\mathbf{k}} = \sum_{u=1}^U \hat{\mathbf{k}}_u$ . Finally, the type is estimated as  $\hat{\mathbf{t}} = \hat{\mathbf{k}} / \|\hat{\mathbf{k}}\|_1$ . The performance of type estimation is evaluated using the average TV distance between the type of the transmitted messages and its estimate, defined as

$$\overline{\text{TV}} = \frac{1}{2} \mathbb{E} \left[ \sum_{m=1}^M |t_m - \hat{t}_m| \right], \quad (3)$$

where the expectation is over the randomness of messages, user positions, small-scale fading, and additive noise.

## III. PROPOSED TUMA DECODER

For the TUMA framework just introduced, we propose a decoder that employs the multisource AMP algorithm developed in [35]. AMP is an iterative algorithm for estimating unknown vectors in large linear systems. In each AMP iteration, a linear residual update is performed, followed by a nonlinear Bayesian denoising operation, together with an Onsager correction that mitigates the correlations created across iterations. This ensures that the effective noise remains Gaussian, which enables accurate asymptotic performance prediction through state evolution [39]. In the multisource AMP framework, the term *multisource* refers to the partitioning of the global codebook into multiple subcodebooks, each treated as a separate signal source. Users are assigned to these sources by selecting the subcodebook corresponding to their LSFCs. The multisource AMP algorithm then processes these sources in parallel within the same iterative procedure. This differs from classical AMP, which operates on a single unpartitioned codebook. The analysis in [35] further establishes that, under Gaussian codebooks, the behavior of multisource AMP in a D-MIMO architecture is accurately predicted by state evolution in the limit  $N_c \rightarrow \infty$  with  $M/N_c$  fixed.

In the TUMA setting, message collisions introduce additional uncertainty: the number of users contributing to each codeword, and their positions within the zone, are both unknown. We account for this by modifying the Bayesian prior so that each unknown effective channel vector  $\mathbf{x}_{u,m}$  is modeled as a weighted mixture over all possible multiplicities and user position distributions within zone  $u$ . Based on this prior, we derive a multiplicity-aware denoiser that computes the posterior mean of the effective channel  $\mathbf{x}_{u,m}$  for each message  $m$ . We also modify the Onsager correction term to ensure consistency with the new denoiser. After the AMP iterations, we estimate the message multiplicities by using their posterior probabilities, computed in the denoising step. The details are provided below.

Throughout, we assume that the receiver has access to the received signal  $\mathbf{Y}$ , the codebook  $\mathbf{C}$ , the transmit energy  $E_c$ , the LSFC model  $\gamma_b(\cdot)$ , and the total number of users  $K$ . However, the decoder treats the number of active users in each zone  $\{K_{a,u}\}_{u \in [U]}$ , as well as their positions, as unknown random variables. Furthermore, no instantaneous channel-state information is available anywhere in the network. In the following, we introduce a centralized decoder and discuss approximations for its efficient implementation. We then propose

a distributed version of this decoder, which is inspired by dAMP [37], which was originally designed for activity detection with perfect per-user LSFC information. Its adaptation to our setting, which involves unknown user positions and message multiplicities, requires nontrivial modifications.

### A. Centralized Decoder

The centralized decoder employs the multisource AMP algorithm [35] to iteratively process the received signal and extract necessary information for multiplicity estimation.

1) *Multisource AMP*: We recap the multisource AMP algorithm from [35] and refer the reader to that work for additional details including its high-dimensional analysis. The algorithm performs  $T_{\text{AMP}}$  iterations, where at iteration  $t$ ,  $\mathbf{X}_u^{(t)}$  denotes the estimate of the effective channel matrix for zone  $u$ , and  $\mathbf{Z}^{(t)}$  denotes the residual noise. These matrices are initialized as  $\mathbf{X}_u^{(0)} = \mathbf{0}$  and  $\mathbf{Z}^{(0)} = \mathbf{Y}$ , and updated as follows

$$\mathbf{R}_u^{(t)} = \mathbf{C}_u^H \mathbf{Z}^{(t-1)} + \sqrt{E_c} \mathbf{X}_u^{(t-1)} \in \mathbb{C}^{M \times F}, \quad (4a)$$

$$\mathbf{X}_u^{(t)} = \eta_{u,t}(\mathbf{R}_u^{(t)}) \in \mathbb{C}^{M \times F}, \quad (4b)$$

$$\mathbf{\Gamma}_u^{(t)} = \mathbf{C}_u \mathbf{X}_u^{(t)} - \frac{M}{N_c} \mathbf{Z}^{(t-1)} \mathbf{Q}_u^{(t)} \in \mathbb{C}^{N_c \times F}, \quad (4c)$$

$$\mathbf{Z}^{(t)} = \mathbf{Y} - \sqrt{E_c} \sum_{u=1}^U \mathbf{\Gamma}_u^{(t)} \in \mathbb{C}^{N_c \times F}. \quad (4d)$$

Here,  $\mathbf{Q}_u^{(t)}$  is the so-called Onsager term [35], which will be described in Section III-A4. The denoiser  $\eta_{u,t}(\cdot)$  acts row-wise on  $\mathbf{R}_u^{(t)}$ . In the large-system limit, where  $N_c \rightarrow \infty$  with  $\alpha \triangleq M/N_c$  and  $E_c$  fixed, state evolution [35] predicts that if  $\mathbf{C}_u \sim_{\text{i.i.d.}} \mathcal{CN}(0, 1/N_c)$ ,<sup>2</sup> each row of  $\mathbf{R}_u^{(t)}$  converges in the high-dimensional sense described in [35] to

$$\mathbf{r}_u^{(t)} = \sqrt{E_c} \mathbf{x}_u + \boldsymbol{\varphi}_u^{(t)}, \quad (5)$$

where  $\mathbf{x}_u$  is a random vector distributed as a generic row of  $\mathbf{X}_u$  and  $\boldsymbol{\varphi}_u^{(t)} \sim \mathcal{CN}(\mathbf{0}, \mathbf{T}^{(t)})$  is the effective noise. We pick the denoiser  $\eta_{u,t}(\cdot)$  as the Bayesian posterior mean estimator (PME) for the model in (5). The covariance matrix  $\mathbf{T}^{(t)}$  evolves according to the state evolution, a recursion that characterizes the AMP algorithm dynamics in the large-system limit [39]. To describe this recursion, we follow [35, Def. 1] and introduce, for each zone  $u$  and iterations  $(t, s)$ , the error-covariance matrices

$$\mathbf{T}_u^{(t,s)} = \alpha E_c \mathbb{E} \left[ (\mathbf{x}_u - \mathbf{x}_u^{(t)}) (\mathbf{x}_u - \mathbf{x}_u^{(s)})^H \right] \in \mathbb{C}^{F \times F}, \quad (6)$$

and the aggregate effective noise covariance

$$\mathbf{T}^{(t,s)} = \sigma_w^2 \mathbf{I}_F + \sum_{u=1}^U \mathbf{T}_u^{(t,s)}. \quad (7)$$

In (6),  $\mathbf{x}_u^{(t)} \triangleq \eta_{u,t}(\sqrt{E_c} \mathbf{x}_u + \boldsymbol{\varphi}_u^{(t)})$ . Note that, by [35, Def. 1],  $\mathbf{T}^{(t,t)}$  is precisely the covariance matrix  $\mathbf{T}^{(t)}$  of

<sup>2</sup>This assumption does not satisfy the deterministic power constraint  $\|\mathbf{c}_{u,m}\|_2^2 = 1$  imposed in Section II-C. However, in our simulations, we have not observed performance differences between Gaussian and normalized Gaussian codebooks under the simulation settings of Section V-A. Therefore, in the numerical results, we employ a normalized Gaussian codebook, obtained by normalizing each Gaussian codeword to unit norm.

$\boldsymbol{\varphi}_u^{(t)}$ . Combining the state evolution equations (6)–(7) with the high-dimensional representation of the AMP residual in [35, Eq. (18)], one can show that, in the large-system limit, using the high-dimensional equivalence introduced in [35] together with the Borel-Cantelli lemma [40, Sec. 4],

$$\frac{1}{N_c} (\mathbf{Z}^{(t-1)})^H \mathbf{Z}^{(t-1)} \xrightarrow{\text{a.s.}} \mathbf{T}^{(t)}, \quad (8)$$

i.e., the empirical covariance of the residual  $\mathbf{Z}^{(t-1)}$  converges almost surely to the effective noise covariance  $\mathbf{T}^{(t)}$ . Because the block diagonal structure in the covariance matrix is preserved by the state evolution recursion [35, Sec. III], we have that  $\mathbf{T}^{(t)} = \text{diag}(\tau_1^{(t)}, \dots, \tau_B^{(t)}) \otimes \mathbf{I}_A$ , where  $\tau_b^{(t)}$  denotes the effective noise variance associated with AP  $b$  at iteration  $t$ . In practice, we estimate these variances from the residual as

$$\tau_b^{(t)} = \frac{1}{AN_c} \sum_{a=1}^A \Re \left\{ [(\mathbf{Z}^{(t-1)})^H \mathbf{Z}^{(t-1)}]_{(b-1)A+a, (b-1)A+a} \right\}, \quad (9)$$

which is a sample-average estimate of the diagonal entries of  $\mathbf{T}^{(t)}$  over the antennas of AP  $b$ . The real-part operator  $\Re\{\cdot\}$  is included as a practical implementation detail to compensate for numerical errors.

2) *Prior Selection*: To derive the PME for the model in (5), we need a prior on  $\mathbf{x}_{u,m}$ . This in turn requires one to specify a prior on the message multiplicities, i.e., a probability distribution  $p(k_{u,m} = k)$ , for  $k = 0, \dots, K$ . This prior is application-dependent, as it is influenced by factors such as the underlying user activity and message selection mechanisms. We provide one such prior for a multi-target localization application in Section IV.

We assume that the active users in each zone  $u$  are independently and uniformly distributed over the zone. Given  $k_{u,m} = k$ , the positions of users transmitting the  $m$ th message in zone  $u$  are denoted by  $\boldsymbol{\rho}_{u,m,1:k} = [\boldsymbol{\rho}_{u,m,1}^T, \dots, \boldsymbol{\rho}_{u,m,k}^T]^T$ , where each  $\boldsymbol{\rho}_{u,m,i}$  is a point in  $\mathcal{D}_u$ .<sup>3</sup> These positions follow the distribution  $p(\boldsymbol{\rho}_{u,m,1:k_{u,m}} | k_{u,m} = k) = 1/|\mathcal{D}_u|^k$ , where  $|\mathcal{D}_u|$  denotes the area of the region  $\mathcal{D}_u$ .

3) *Denoiser*: The Bayesian PME of  $\mathbf{x}_{u,m}$  given  $\mathbf{R}_u^{(t)}$  is derived using the large-system approximation (5). For simplicity, the iteration index  $(t)$  is omitted in the following equations. We can express the PME denoiser as

$$\eta_u(\mathbf{r}_{u,m}) = \sum_{k=1}^K \mathbb{E}[\mathbf{x}_{u,m} | \mathbf{r}_{u,m}, k_{u,m} = k] p(k_{u,m} = k | \mathbf{r}_{u,m}). \quad (10)$$

We next compute both terms on the right-hand side (RHS) of (10). For notational simplicity, we omit the subscript  $m$  and use  $k_u$ ,  $\boldsymbol{\rho}_{u,1:k_u}$ ,  $\mathbf{r}_u$ , and  $\mathbf{x}_u$  to denote  $k_{u,m}$ ,  $\boldsymbol{\rho}_{u,m,1:k_{u,m}}$ ,  $\mathbf{r}_{u,m}$ , and  $\mathbf{x}_{u,m}$ , respectively. Using Bayes' theorem, we can express the second factor on the RHS of (10) as

$$p(k_u = k | \mathbf{r}_u) = \frac{p(\mathbf{r}_u | k_u = k) p(k_u = k)}{\sum_{\ell=0}^K p(\mathbf{r}_u | k_u = \ell) p(k_u = \ell)}. \quad (11)$$

<sup>3</sup>We treat all positions as 2D coordinates for simplicity. An extension to 3D coordinates is straightforward.

The likelihood  $p(\mathbf{r}_u | k_u = k)$  is given by

$$\begin{aligned} p(\mathbf{r}_u | k_u = k) &= \int_{\mathcal{D}_u^k} p(\mathbf{r}_u | \boldsymbol{\rho}_{u,1:k}, k_u = k) p(\boldsymbol{\rho}_{u,1:k} | k_u = k) d\boldsymbol{\rho}_{u,1:k} \\ &= \frac{1}{|\mathcal{D}_u^k|} \int_{\mathcal{D}_u^k} p(\mathbf{r}_u | \boldsymbol{\rho}_{u,1:k}) d\boldsymbol{\rho}_{u,1:k}, \end{aligned} \quad (12a)$$

$$= \frac{1}{|\mathcal{D}_u^k|} \int_{\mathcal{D}_u^k} p(\mathbf{r}_u | \boldsymbol{\rho}_{u,1:k}) d\boldsymbol{\rho}_{u,1:k}, \quad (12b)$$

where  $\mathcal{D}_u^k = \mathcal{D}_u \times \dots \times \mathcal{D}_u$ . In (12a), we used the law of total probability, and in (12b), we used the Markov property  $k_u \leftrightarrow \boldsymbol{\rho}_{u,1:k_u} \leftrightarrow \mathbf{x}_u \leftrightarrow \mathbf{r}_u$  and the assumption that  $p(\boldsymbol{\rho}_{u,1:k_u} | k_u = k) = 1/|\mathcal{D}_u^k|$ . It follows from (1) and (5) that, in the large-system limit and for the case  $k_u = k$ , the likelihood  $p(\mathbf{r}_u | \boldsymbol{\rho}_{u,1:k})$  is given by

$$p(\mathbf{r}_u | \boldsymbol{\rho}_{u,1:k}) = \mathcal{CN}(\mathbf{r}_u; \mathbf{0}, \mathbf{T} + \mathbb{E}_c \sum_{i=1}^k \Sigma(\boldsymbol{\rho}_{u,i})). \quad (13)$$

Next, the conditional mean  $\mathbb{E}[\mathbf{x}_u | \mathbf{r}_u, k_u = k]$  in (10) can be expressed as

$$\begin{aligned} \mathbb{E}[\mathbf{x}_u | \mathbf{r}_u, k_u = k] &= \int_{\mathcal{D}_u^k} \mathbb{E}[\mathbf{x}_u | \mathbf{r}_u, \boldsymbol{\rho}_{u,1:k}] p(\boldsymbol{\rho}_{u,1:k} | \mathbf{r}_u) d\boldsymbol{\rho}_{u,1:k}. \end{aligned} \quad (14)$$

Note now that (5), together with the Gaussianity of  $\mathbf{x}_u$ , imply that [41, Sec. 12.5]

$$\begin{aligned} \mathbb{E}[\mathbf{x}_u | \mathbf{r}_u, \boldsymbol{\rho}_{u,1:k}] &= (\sqrt{\mathbb{E}_c} \sum_{i=1}^k \Sigma(\boldsymbol{\rho}_{u,i})) (\mathbf{T} + \mathbb{E}_c \sum_{i=1}^k \Sigma(\boldsymbol{\rho}_{u,i}))^{-1} \mathbf{r}_u. \end{aligned} \quad (15)$$

Finally, we evaluate the posterior of the user positions in (14) as

$$\begin{aligned} p(\boldsymbol{\rho}_{u,1:k} | \mathbf{r}_u) &= p(\boldsymbol{\rho}_{u,1:k_u} | \mathbf{r}_u, k_u = k) \\ &= \frac{p(\mathbf{r}_u | \boldsymbol{\rho}_{u,1:k_u}, k_u = k) p(\boldsymbol{\rho}_{u,1:k_u} | k_u = k)}{p(\mathbf{r}_u | k_u = k)} \end{aligned} \quad (16a)$$

$$= \frac{p(\mathbf{r}_u | \boldsymbol{\rho}_{u,1:k}) p(\boldsymbol{\rho}_{u,1:k})}{\int_{\mathcal{D}_u^k} p(\mathbf{r}_u | \boldsymbol{\rho}'_{u,1:k}) p(\boldsymbol{\rho}'_{u,1:k} | k_u = k) d\boldsymbol{\rho}'_{u,1:k}} \quad (16b)$$

$$= \frac{p(\mathbf{r}_u | \boldsymbol{\rho}_{u,1:k}) / |\mathcal{D}_u|^k}{\int_{\mathcal{D}_u^k} (p(\mathbf{r}_u | \boldsymbol{\rho}'_{u,1:k}) / |\mathcal{D}_u|^k) d\boldsymbol{\rho}'_{u,1:k}} \quad (16c)$$

$$= \frac{p(\mathbf{r}_u | \boldsymbol{\rho}_{u,1:k})}{\int_{\mathcal{D}_u^k} p(\mathbf{r}_u | \boldsymbol{\rho}'_{u,1:k}) d\boldsymbol{\rho}'_{u,1:k}}. \quad (16d)$$

Here, (16a) follows from the Bayes' theorem, (16b) from the law of total probability and the Markov property  $k_u \leftrightarrow \boldsymbol{\rho}_{u,1:k_u} \leftrightarrow \mathbf{x}_u \leftrightarrow \mathbf{r}_u$ , and (16c) from the assumption of a uniform prior.

4) *Onsager Correction:* In multisource AMP [35], the Onsager term  $\mathbf{Q}_u^{(t)} \in \mathbb{C}^{\mathbb{F} \times \mathbb{F}}$  in (4c) is given by

$$[\mathbf{Q}_u^{(t)}]_{a,b} = \frac{1}{M} \sum_{m=1}^M \frac{\partial [\eta_{u,t}(\mathbf{r}_{u,m})]_b}{\partial [\mathbf{r}_{u,m}]_a}. \quad (17)$$

A numerically computable expression for this term is provided in Appendix A.

5) *Multiplicity Estimation:* We perform maximum a posteriori decoding as

$$\hat{k}_{u,m} = \arg \max_{k \in \{0,1,\dots,K\}} p(k_{u,m} = k | \mathbf{r}_{u,m}). \quad (18)$$

Then, we estimate the type  $\hat{\mathbf{t}}$  as outlined in Section II-D.

---

### Algorithm 1 Centralized Decoder with Monte Carlo Sampling

**Inputs:** Received signal  $\mathbf{Y}$ , codebook  $\mathbf{C}$ , transmit energy  $\mathbb{E}_c$ , sampled positions  $\{\boldsymbol{\rho}_{u,1:k}^i\}_{i=1}^{\text{NMC}}$  for all  $k \in [K_{\max}]$ ,  $u \in [U]$

**Output:** Estimated type vector  $\hat{\mathbf{t}}$

**Initialization:**  $\mathbf{Z}^{(0)} = \mathbf{Y}$ ,  $\mathbf{X}_u^{(0)} = \mathbf{0}$ , for all  $u \in [U]$

#### 1. AMP for Channel Estimation:

- 1: Precompute  $\{\sum_{j=1}^k \Sigma(\boldsymbol{\rho}_{u,j}^i)\}_{i=1}^{\text{NMC}}$  for  $k \in [K_{\max}]$ ,  $u \in [U]$
- 2: **for**  $t \leftarrow 1$  to  $T_{\text{AMP}}$  **do**
- 3:   **for**  $u \leftarrow 1$  to  $U$  **do**
- 4:      $\mathbf{R}_u^{(t)} \leftarrow \mathbf{C}_u^H \mathbf{Z}^{(t-1)} + \sqrt{\mathbb{E}_c} \mathbf{X}_u^{(t-1)}$
- 5:     Compute  $\mathbf{T}^{(t)}$  as in (9)
- 6:      $\mathbf{X}_u^{(t)} \leftarrow \eta_{u,t}(\mathbf{R}_u^{(t)})$  using (10)-(16), (20) and (19)
- 7:     Compute  $\mathbf{Q}_u^{(t)}$  as in (17) and Appendix A
- 8:      $\Gamma_u^{(t)} \leftarrow \mathbf{C}_u \mathbf{X}_u^{(t)} - \frac{M}{N_c} \mathbf{Z}^{(t-1)} \mathbf{Q}_u^{(t)}$
- 9:   **end for**
- 10:    $\mathbf{Z}^{(t)} \leftarrow \mathbf{Y} - \sqrt{\mathbb{E}_c} \sum_{u=1}^U \Gamma_u^{(t)}$
- 11: **end for**

#### 2. Type Estimation:

- 12: Estimate  $\{\hat{k}_u\}_{u \in [U]}$  as in (18) using  $p(k_{u,m} = k | \mathbf{r}_{u,m})$  computed in line 6 with (19)
  - 13:  $\hat{\mathbf{t}} \leftarrow \sum_{u=1}^U \hat{k}_u / \|\sum_{u=1}^U \hat{k}_u\|_1$
- 

### B. Approximations for Efficient Implementation

The PME denoiser involves multi-dimensional integrals in (12b), (14), and (16d) whose evaluation becomes computationally prohibitive for large values of multiplicities. One could discretize the coverage area using a uniform discrete grid. However, the complexity of this approach still grows exponentially with the multiplicity. Instead, we adopt MC sampling. Specifically, we draw user positions independently from the uniform prior over  $\mathcal{D}_u$ . Let  $\{\boldsymbol{\rho}_{u,1:k}^i\}_{i=1}^{\text{NMC}}$  denote the MC samples of the positions of  $k$  users. Using these samples, we approximate (11) as

$$p(k_u = k | \mathbf{r}_u) \approx \frac{\sum_{i=1}^{\text{NMC}} p(\mathbf{r}_u | \boldsymbol{\rho}_{u,1:k}^i) p(k_u = k)}{\sum_{i=1}^{\text{NMC}} \sum_{\ell=0}^K p(\mathbf{r}_u | \boldsymbol{\rho}_{u,1:\ell}^i) p(k_u = \ell)}. \quad (19)$$

and (14) as

$$\mathbb{E}[\mathbf{x}_u | \mathbf{r}_u, k_u = k] \approx \frac{\sum_{i=1}^{\text{NMC}} \mathbb{E}[\mathbf{x}_u | \mathbf{r}_u, \boldsymbol{\rho}_{u,1:k}^i] p(\mathbf{r}_u | \boldsymbol{\rho}_{u,1:k}^i)}{\sum_{i=1}^{\text{NMC}} p(\mathbf{r}_u | \boldsymbol{\rho}_{u,1:k}^i)}. \quad (20)$$

To further reduce complexity, we limit the computation to a maximum multiplicity  $K_{\max}$ , i.e., we replace  $K$  in equations (10), (11), (18), and (20) by  $K_{\max}$ . The choice of  $K_{\max}$  can be guided by the prior  $p(k_{u,m} = k)$ , to ensure that only statistically significant multiplicities are considered. We summarize the proposed centralized decoder with MC sampling-based approximation in Algorithm 1.

### C. Distributed Decoder

To improve scalability in D-MIMO systems [42], we propose a distributed decoder inspired by dAMP [37]. Rather than assuming that the received signal is entirely processed at the CPU, we consider a scenario in which each AP locally

processes its received signal and transmits the likelihoods of each codeword to the CPU. Then, the likelihoods are aggregated as (see Appendix B)

$$p(\mathbf{r}_{u,m} | \boldsymbol{\rho}_{u,1:k}) = \prod_{b=1}^B p_b(\mathbf{r}_{b,u,m} | \boldsymbol{\rho}_{u,1:k}), \quad (21)$$

where  $p_b(\mathbf{r}_{b,u,m} | \boldsymbol{\rho}_{u,1:k})$  is the local likelihood computed at AP  $b$  with MC sampling as in (19). The posterior probability is then computed as

$$p(k_{u,m} = k | \mathbf{r}_{u,m}) = \frac{p(k_{u,m} = k) \prod_{b=1}^B p_b(\mathbf{r}_{b,u,m} | \boldsymbol{\rho}_{u,1:k})}{\sum_{\ell=0}^K p(k_{u,m} = \ell) \prod_{b=1}^B p_b(\mathbf{r}_{b,u,m} | \boldsymbol{\rho}_{u,1:\ell})}. \quad (22)$$

as detailed in Appendix B. This design improves scalability by reducing the CPU's workload through local processing at APs. As before, we can replace  $K$  with  $K_{\max}$  in (22). The CPU then performs posterior computation and type estimation following the steps already detailed in Section III-A.

#### D. Complexity Analysis

The per-iteration complexity of the centralized decoder is dominated by two operations: (i) the linear AMP updates involve multiplications by  $\mathbf{C}_u$  and  $\mathbf{C}_u^H$  across all zones, which scale as  $O(\bar{M} \cdot N_c)$ ; (ii) the PME denoising operation, which involves, for each of the  $\bar{M}$  codewords,  $N_{\text{MC}}$  MC samples for each of the at most  $K$  multiplicity hypotheses and  $F$  receive antennas. Because the posterior covariances are diagonal, each likelihood evaluation is  $O(F)$ , leading to  $O(\bar{M} \cdot N_{\text{MC}} \cdot K \cdot F)$  operations. Combining these terms, we obtain a complexity of order  $O(\bar{M} \cdot (N_c + N_{\text{MC}} \cdot K \cdot F))$ . By limiting the analysis to a maximum multiplicity  $K_{\max}$ , we can reduce the complexity to  $O(\bar{M} \cdot (N_c + N_{\text{MC}} \cdot K_{\max} \cdot F))$ .

In the distributed decoder, each AP operates on a subset of the data, reducing the per-device computational load. Specifically, the per-AP complexity is of order  $O(\bar{M} \cdot (N_c + N_{\text{MC}} \cdot K_{\max} \cdot A))$ . After local processing, the CPU aggregates the likelihoods and performs type estimation with complexity  $O(\bar{M} \cdot B)$ . Since  $A \ll F$  in typical D-MIMO systems, the distributed approach reduces significantly the computational cost.

## IV. MULTI-TARGET LOCALIZATION WITH TUMA

We apply the TUMA framework proposed in Sections II and III to a multi-target localization scenario with  $K$  sensors and  $T$  targets in the coverage area  $\mathcal{D}$ . The sensors, which act as users, aim to detect the targets and report their positions to the APs using TUMA. The target positions are denoted as  $\mathcal{T} = \{\mathbf{p}_1, \dots, \mathbf{p}_T\} \in \mathcal{D}^T$ , and the sensor positions as  $\mathcal{S} = \{\mathbf{s}_1, \dots, \mathbf{s}_K\} \in \mathcal{D}^K$ . Each sensor detects the targets using a probabilistic sensing model and quantizes the positions of the detected targets before transmission. Throughout, we assume that each sensor may report at most a single target position: if more than one target is detected, the sensor reports only the closest detected target. We now detail each step of the multi-target localization framework.

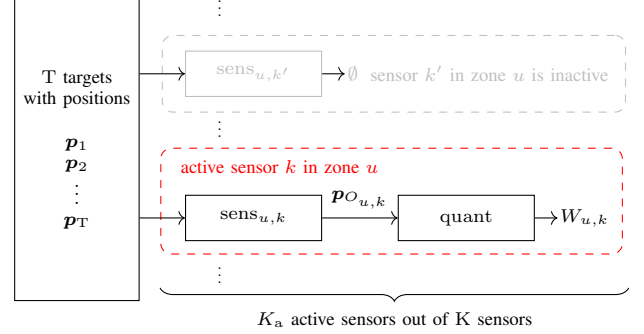


Fig. 3. Block diagram for message generation process in multi-target localization with TUMA.

#### A. Sensor Activation and Message Generation

We define the sensing function for sensor  $j$  in zone  $u$  as  $\text{sens}_{u,j} : \mathcal{D}^T \rightarrow \mathcal{D} \cup \{\emptyset\}$ . It operates as follows:

- $\text{sens}_{u,j}(\mathcal{T}) = \emptyset$  indicates that the sensor  $(u, j)$  does not detect any target and therefore remains inactive.
- $\text{sens}_{u,j}(\mathcal{T}) = \mathbf{p}_{O_{u,j}}$  means that the sensor  $(u, j)$  detects a target at position  $\mathbf{p}_{O_{u,j}} \in \mathcal{D}$ , where  $O_{u,j} \in [T]$  denotes the index of the detected target.

We denote by  $K_{a,u}$  the number of active sensors in zone  $u$ , i.e., the number of sensors that detect a target. Without loss of generality, we assume that active sensors in zone  $u$  occupy the first  $K_{a,u}$  indices. That is, we reorder sensor indices so that  $\text{sens}_{u,j}(\mathcal{T}) \neq \emptyset, \forall j \leq K_{a,u}$  and  $\text{sens}_{u,j}(\mathcal{T}) = \emptyset, \forall j > K_{a,u}$ . This simplifies notation and allows us to directly index the active sensors in zone  $u$  as  $(u, k)$  with  $k \in [K_{a,u}]$ .

Each active sensor then quantizes the detected target position using a predefined quantization codebook  $\mathcal{Q} = \{\mathbf{q}_1, \dots, \mathbf{q}_M\} \subset \mathcal{D}$ . The quantization function is defined as  $\text{quant} : \mathcal{D} \rightarrow [M]$  with  $\text{quant}(\mathbf{p}_{O_{u,k}}) = W_{u,k}$ . The index  $W_{u,k}$  is the message transmitted by the active sensor  $(u, k)$  in the TUMA communication framework. A block diagram illustrating this message generation process is shown in Fig. 3.

#### B. Sensing Model

We adopt a probabilistic sensing model based on mmWave 5G SLAM to capture realistic sensing dynamics. Specifically, sensors transmit orthogonal frequency division multiplexing (OFDM) pilot signals to detect targets via reflected signals. Using the sensing formulation in [38], we model the probability that a sensor at position  $\mathbf{s}$  detects a target at position  $\mathbf{p}$  as

$$p_d(\mathbf{s}, \mathbf{p}) = Q_1 \left( \sqrt{\frac{2N_s P_s S \lambda^2}{(4\pi)^3 P_n \|\mathbf{s} - \mathbf{p}\|^4}}, \sqrt{\gamma} \right). \quad (23)$$

Here,  $Q_1(\cdot, \cdot)$  is the Marcum-Q function of order 1,  $N_s$  is the number of OFDM symbols used for sensing, referred to as sensing blocklength, and  $P_s$  is the per-symbol transmit power allocated for sensing. In addition,  $S$  corresponds to the radar cross-section of the target, while  $\lambda$  denotes the signal wavelength, computed as the speed of light divided by the carrier frequency  $f_c$ . The parameter  $P_n$  represents the thermal noise power. The threshold  $\gamma$  determines the false

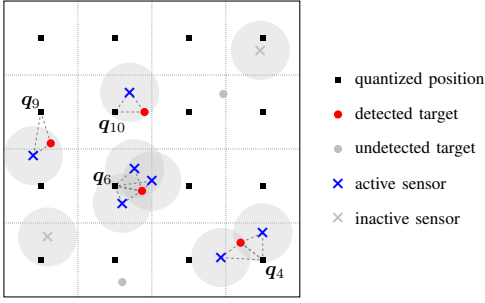


Fig. 4. An example of multi-target position localization in a square with  $T = 6$  targets, of which  $T_d = 3$  are detected,  $K = 9$  sensors, of which  $K_a = 7$  are active, and  $M = 16$  quantized positions. Circles around sensors depict their detection range.

alarm probability according to  $p_{fa} = e^{-\gamma/2}$  [38, Eq. (8)]. Finally, to simplify the analysis, we assume that, while targets can be misdetections, sensors can perfectly localize the detected targets, leveraging the high-resolution capabilities of mmWave sensing [43]–[45].

### C. Quantization Model

We employ a fixed uniform quantization over the region  $\mathcal{D}$ , without optimizing the quantization points. Specifically, we assume that the quantized positions define a regular grid within  $\mathcal{D}$ . Each active sensor  $(u, k)$  maps the detected target position  $\mathbf{p}_{O_{u,k}}$  to the nearest point in the quantization codebook  $\mathcal{Q}$  in Euclidean distance:

$$W_{u,k} = \text{quant}(\mathbf{p}_{O_{u,k}}) = \arg \min_{m \in [M]} \|\mathbf{q}_m - \mathbf{p}_{O_{u,k}}\|. \quad (24)$$

In Fig. 4, we illustrate an example of the sensing and quantization process, showing target locations, sensor detections along with their corresponding detection regions, and uniform quantization grids. Note that this figure complements Fig. 1, which shows zone partitioning and AP placements.

### D. Prior Computation

We next describe the prior that will be used in the Bayesian PME (see Section III-A2).

1) *Sensor Activation Probability*: A sensor becomes active if it detects at least one target. For a sensor at position  $\mathbf{s}$ , the activation probability is given by

$$p_{\text{active}}(\mathbf{s}) = 1 - \frac{1}{|\mathcal{D}|^T} \int_{\mathcal{D}^T} \prod_{i=1}^T (1 - p_d(\mathbf{s}, \mathbf{p}_i)) d\mathbf{p}_{1:T}, \quad (25)$$

where  $\mathbf{p}_{1:T} = \{\mathbf{p}_1, \dots, \mathbf{p}_T\}$  denote the target positions and  $p_d(\cdot, \cdot)$  is the detection probability in (23). Averaging over all possible sensor locations, we conclude that the sensor activation probability is

$$p_{\text{active}} = \frac{1}{|\mathcal{D}|} \int_{\mathcal{D}} p_{\text{active}}(\mathbf{s}) d\mathbf{s}. \quad (26)$$

The number of active sensors  $K_a$  then follows a  $\text{Bin}(K, p_{\text{active}})$  distribution.

2) *Distribution of Active Sensors in Zones*: Assuming a uniform sensor placement and equal-area zones, we conclude that the number of active sensors in zone  $u$ , denoted by  $K_{a,u}$ , follows a binomial distribution  $\text{Bin}(K_a, 1/U)$  given  $K_a$ . Marginalizing over  $K_a$ , we obtain

$$p(K_{a,u} = k) = \sum_{K_a=0}^K \text{Bin}(k; K_a, 1/U) \text{Bin}(K_a; K, p_{\text{active}}). \quad (27)$$

3) *Message Selection Probability*: Each active sensor reports the closest detected target. For a sensor at position  $\mathbf{s}$ , the probability that a target at position  $\mathbf{p}$  is the closest among the detected ones is

$$p_{\text{closest}}(\mathbf{s}, \mathbf{p}) = \frac{1}{|\mathcal{D}|^{T-1}} \int_{\mathcal{D}^{T-1}} \prod_{\mathbf{p}'_i \neq \mathbf{p}} (1 - p_d(\mathbf{s}, \mathbf{p}'_i)) \cdot \mathbb{1}\{\|\mathbf{s} - \mathbf{p}'_i\| < \|\mathbf{s} - \mathbf{p}\|\} d\mathbf{p}'_{1:T-1}. \quad (28)$$

Let  $\mathcal{R}_m = \{\mathbf{p} \in \mathcal{D} : \|\mathbf{q}_m - \mathbf{p}\| \leq \|\mathbf{q}_{m'} - \mathbf{p}\|, \forall m' \in [M], m' \neq m\}$  denote the Voronoi region associated with the center point  $\mathbf{q}_m$ . The probability that an active sensor at position  $\mathbf{s}$  in zone  $u$  selects the message index  $m$  is given by

$$p(m \mid \text{sensor in zone } u) = \frac{1}{|\mathcal{D}|} \frac{1}{|\mathcal{D}_u|} \int_{\mathcal{D}_u} \int_{\mathcal{R}_m} p_d(\mathbf{s}, \mathbf{p}) p_{\text{closest}}(\mathbf{s}, \mathbf{p}) d\mathbf{p} d\mathbf{s}. \quad (29)$$

4) *Prior for Local Multiplicities*: Given  $K_{a,u}$  active users in zone  $u$ , the local multiplicities  $k_{u,m}$  follow a  $\text{Bin}(K_{a,u}, p(m \mid \text{sensor in zone } u))$  distribution. By marginalizing over  $K_a$  and  $K_{a,u}$ , we obtain the prior as

$$p(k_{u,m} = k) = \sum_{K_a=0}^K \sum_{K_{a,u}=0}^{K_a} \text{Bin}(k; K_{a,u}, p(m \mid \text{sensor in zone } u)) \cdot \text{Bin}(K_{a,u}; K_a, 1/U) \text{Bin}(K_a; K, p_{\text{active}}). \quad (30)$$

### E. Performance Metrics

We evaluate the performance of the proposed TUMA-based multi-target localization system using metrics that capture the impact of sensing, quantization, and communication. To this end, we consider four complementary metrics:

1) *TV Distance*: The TV distance, introduced in (3), measures the error in estimating the type. This metric characterizes only communication performance, and does not account for sensing misdetections and quantization distortion.

2) *Wasserstein Distance*: Let  $\ell = [\ell_1, \dots, \ell_T]$ , where  $\ell_i = \sum_{u=1}^U \sum_{j=1}^{K_u} \mathbb{1}\{O_{u,j} = i\}$  is the number of sensors that detect target  $i \in [T]$ , and define the corresponding type as  $\omega = \ell/K_a$ . We can then define the empirical distribution associated with the true target positions as  $\mu = \sum_{i=1}^T \omega_i \delta(\mathbf{p}_i)$  and its estimate at the receiver as  $\hat{\mu} = \sum_{j=1}^M \hat{\ell}_j \delta(\mathbf{q}_j)$ .

To capture both quantization and communication errors, we consider the metric

$$\overline{\mathbb{W}}_p = \mathbb{E}[\mathbb{W}_p(\mu, \hat{\mu})], \quad (31)$$

where the expectation is over the random target and sensor positions, small-scale fading, and additive noise. Here,  $\mathbb{W}_p(\cdot, \cdot)$  is the  $p$ -Wasserstein distance [46, Chap. 2] defined as

$$\mathbb{W}_p(\mu, \hat{\mu}) = \inf_{e_{i,j} \in [0,1]} \left( \sum_{i=1}^T \sum_{j=1}^M e_{i,j} \| \mathbf{p}_i - \mathbf{q}_j \|_p^p \right)^{1/p}$$

subject to  $\sum_{i=1}^T e_{i,j} = \hat{t}_j, \sum_{j=1}^M e_{i,j} = \omega_i.$

(32)

This metric captures the mismatch between true and estimated types through an optimal transport formulation. This distance and its generalizations have been widely used in multi-target localization [20]–[22].

3) *Empirical Misdetction Probability*: Let  $\mathcal{T}_d = \{ \mathbf{p}_i \in \mathcal{T} : \omega_i > 0 \}$  denote the set of detected targets and let  $T_d = |\mathcal{T}_d|$ . The empirical misdetction probability is defined as

$$p_{\text{md}} = \mathbb{E} \left[ \frac{|\mathcal{T} \setminus \mathcal{T}_d|}{|\mathcal{T}|} \right] = 1 - \frac{\mathbb{E}[T_d]}{T}. \quad (33)$$

This metric isolates the sensing errors by quantifying the average fraction of undetected targets.

4) *GOSPA-Like Cost*: To capture in a single metric the impact of sensing and communication errors, as well as quantization effects, we define the following cost function

$$d^{(c,p)} = \mathbb{E} \left[ (\mathbb{W}_p(\mu, \hat{\mu})^p + c^p (1 - T_d/T))^{1/p} \right], \quad (34)$$

which extends the GOSPA metric [22] by replacing its assignment-based localization term in [22] with a Wasserstein distance and incorporating misdetection cost via the  $1 - T_d/T$  term. The parameter  $c$  governs the tradeoff between localization errors for detected targets and misdetection probability, while  $p$  determines how strongly large localization errors influence the overall cost.

## V. SIMULATION RESULTS AND DISCUSSION

### A. Simulation Setup

We consider a D-MIMO system in which  $B = 40$  APs are deployed to form a  $3 \times 3$  square grid layout over a square coverage area, as illustrated in Fig. 1. Each AP is equipped with  $A = 4$  antennas, leading to  $F = 160$  receive antennas in total. Following the setup in [35], we model the LSFC as  $\gamma_b(\rho) = 1/(1 + (\|\rho - \nu_b\|/d_0)^\beta)$ , where  $\nu_b$  denotes the position of AP  $b$ , the path-loss exponent is  $\beta = 3.67$  and the 3 dB cutoff distance is  $d_0 = 13.57$  m. The side length of each zone is set to 100 m. The AP placement together with the LSFC model induce a partition of the coverage area into  $3 \times 3$  nonoverlapping square zones, resulting in  $U = 9$  zones. As in [35], we define the received SNR as  $\text{SNR}_{\text{rx}} = \text{SNR}_{\text{tx}}/(1 + (\zeta/d_0)^\alpha)$ , where  $\zeta = 50$  m denotes the distance between a zone centroid (green dot in Fig. 1) and its closest AP. The codewords  $\{ \mathbf{c}_{u,m} \}$  are independently generated by first sampling each entry independently from a Gaussian distribution  $\mathcal{CN}(0, 1/N_c)$ , and then normalizing each codeword such that  $\|\mathbf{c}_{u,m}\|_2^2 = 1$ . The number of MC samples used in the multisource AMP decoder is set to  $N_{\text{MC}} = 500$ . We run the decoder for  $T_{\text{AMP}} = 10$  iterations. We obtain

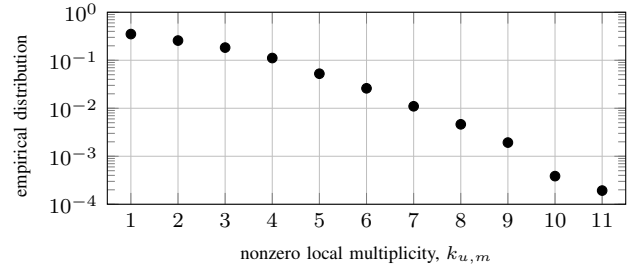


Fig. 5. Empirical distribution of nonzero local multiplicities for the multi-target localization scenario described in Section V-A. Here, we consider  $T = 50$  targets,  $K = 200$  sensors,  $\log_2 M = 10$  bits, and a sensing blocklength  $N_s = 1000$ .

all reported performance metrics by averaging over 100 independent MC simulation runs, with independent realizations of user positions, target positions, small-scale fading, and additive noise.<sup>4</sup>

We evaluate the performance of the proposed TUMA framework in the multi-target localization setting. A total of  $T = 50$  targets and  $K = 200$  sensors are independently and uniformly placed over the coverage area  $\mathcal{D}$  in each simulation run. All performance results are averaged over 100 independent simulations. For simulations involving the Wasserstein distance (32) and the GOSPA-like cost function (34), we set the exponent  $p = 2$ , which corresponds to the commonly used Euclidean metric. The weight parameter  $c$  is chosen to ensure that a single misdetection is equivalent in terms of cost to a localization error where the distance between true and estimated positions coincides the distance between adjacent quantization points under a 6-bit resolution. For our  $300 \text{ m} \times 300 \text{ m}$  area, this results in  $c = 300/\sqrt{2^6} = 37.5$  m.

The sensing parameters in the target detection probability in (23) are set as follows: the radar cross-section area is  $S = 10 \text{ m}^2$ , the carrier frequency is  $f_c = 28 \text{ GHz}$ , and thermal noise power is  $P_n = 10^{-8} \text{ Watts}$ .<sup>5</sup> The per-symbol sensing power is set equal to the communication power  $P_s = E_c/N_c = 1 \text{ mW}$ . The detection threshold is set to  $\gamma = 36.84$ , corresponding to a false alarm probability  $p_{\text{fa}} = 10^{-8}$ . In the simulations, false alarms are ignored.

The total blocklength  $N$  is shared between sensing and communication as  $N = N_s + N_c$ , according to a time-division resource allocation strategy. Similar time-sharing models have been widely adopted in the literature to characterize tradeoffs under limited resources [47]–[49]. Unless stated otherwise, we assume  $N = 2000$ , with an equal allocation of resources for sensing and communication, i.e.,  $N_s = N_c = 1000$ .

### B. Results

We start by verifying that, for the scenario described in Section V-A, it is likely that sensors within the same zone

<sup>4</sup>The simulation code is available at [https://github.com/okumuskaan/tuma\\_mtl](https://github.com/okumuskaan/tuma_mtl) to support reproducible research.

<sup>5</sup>These parameter values are chosen to reflect a typical mmWave setting. The noise power  $P_n = 10^{-8} \text{ W}$  corresponds to a 200 MHz bandwidth and a noise power spectral density of  $-174 \text{ dBm/Hz}$ . A radar cross-section of  $10 \text{ m}^2$  models medium-sized targets, and  $f_c = 28 \text{ GHz}$  is a commonly chosen carrier frequency in mmWave sensing applications.

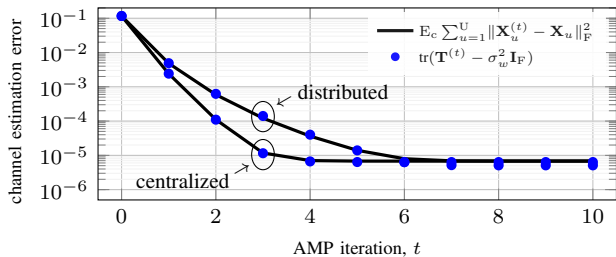


Fig. 6. Channel estimation error vs. multisource AMP iteration for  $\text{SNR}_{\text{rx}} = 10$  dB,  $N_c = N_s = 1000$ , and  $M = 2^{10}$ .

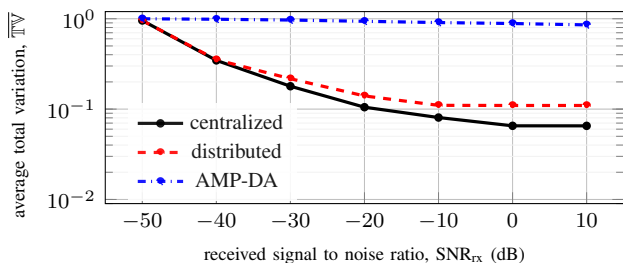


Fig. 7. The average total variation  $\overline{\mathbb{T}\mathbb{V}}$  vs. received signal to noise ratio  $\text{SNR}_{\text{rx}}$  for  $N_s = N_c = 1000$ , and  $M = 2^{10}$ .

transmit the same codewords, resulting in local multiplicities  $k_{u,m} > 1$ , which, in turn, justifies the need for the proposed TUMA framework. Notably, as shown in Fig. 5, more than 70% of the transmitted codewords are involved in collisions, i.e., they are transmitted by multiple sensors.

To validate the modified multisource AMP decoder, we analyze the convergence behavior of the estimated effective channel matrix  $\mathbf{X}$ . As shown in Fig. 6, both centralized and distributed AMP decoders exhibit fast convergence, typically within  $t = 6$  iterations. This aligns with the state evolution result in [35, Eq. (79)], which predicts that the estimation error  $E_c \sum_{u=1}^U \|\mathbf{X}_u^{(t)} - \mathbf{X}_u\|_F^2$  converges to  $\text{tr}(\mathbf{T}^{(t)} - \sigma_w^2 \mathbf{I}_F)$  in the large-system limit, where  $N_c \rightarrow \infty$  with  $M/N_c$  fixed.

In Fig. 7, we evaluate the type estimation performance in terms of  $\overline{\mathbb{T}\mathbb{V}}$  defined in (3) as a function of  $\text{SNR}_{\text{rx}}$ . As expected, higher  $\text{SNR}_{\text{rx}}$  results in lower  $\overline{\mathbb{T}\mathbb{V}}$  values, and hence, higher estimation accuracy. The centralized decoder performs slightly better, whereas the distributed decoder offers competitive accuracy with better scalability. We further compare our decoders with AMP-DA [23], which let the users pre-equalize the channel to obtain an effective AWGN channel model, and then apply scalar AMP [31, Sec. IV-C] for type estimation. We emphasize that the pre-equalization step relies on the availability of CSI at the users. Our decoders instead do not require CSI, neither at the users nor the receiver. In our AMP-DA simulations, we normalize the transmitted signal so that the transmit communication power is 1 mW. As shown in Fig. 7, for the received SNR values considered in the figure, AMP-DA results in much higher  $\overline{\mathbb{T}\mathbb{V}}$  than the two TUMA decoders.

In Fig. 8, we explore the tradeoff between sensing and communication under a total blocklength of  $N = 2000$ , with  $\log_2 M = 10$  bits and  $\text{SNR}_{\text{rx}} = 10$  dB. We vary the sensing blocklength  $N_s$  from 10 to 1900 and observe the resulting performance trends. As shown in Fig. 8(a), increasing the number of sensing symbols  $N_s$  improves detection reliability,

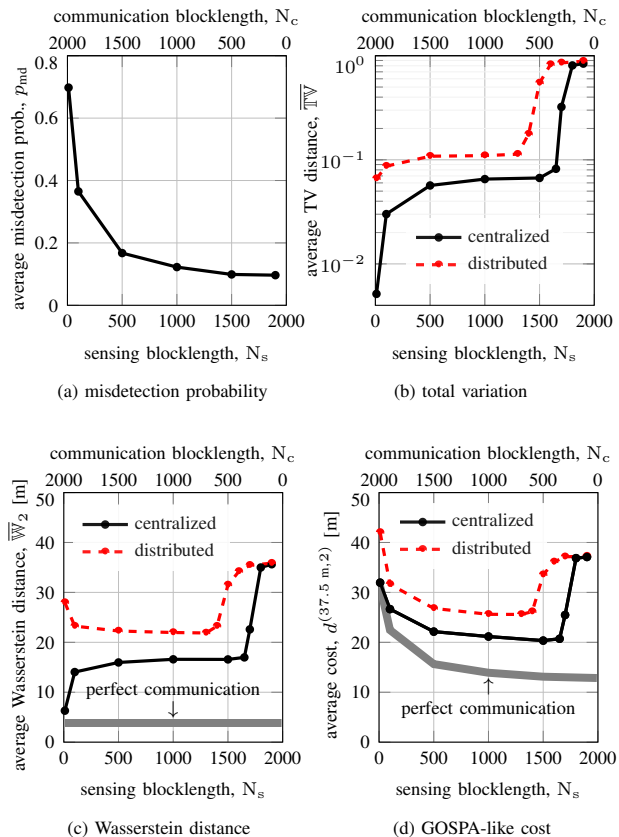


Fig. 8. Performance results vs. sensing blocklength  $N_s$  for  $K = 200$  sensors,  $T = 50$  targets,  $\text{SNR}_{\text{rx}} = 10$  dB, and  $M = 2^{10}$  messages. The total blocklength is  $N = 2000$ , with communication blocklength  $N_c = N - N_s$ .

leading to a lower empirical misdetection probability. However, this comes at the cost of fewer symbols available for communication, which limits the decoder's ability to distinguish between messages. This degradation is evident in the rising total variation distance  $\overline{\mathbb{T}\mathbb{V}}$  in Fig. 8(b). The Wasserstein distance  $\overline{\mathbb{W}}_2$  in Fig. 8(c), which captures average localization error over detected targets, exhibits a similar trend: improved detection at small  $N_s$  is offset by rising communication errors at large values. The GOSPA-like cost in Fig. 8(d) integrates all three aspects: sensing, quantization, and communication, to provide a unified performance measure. It reveals a clear tradeoff with a minimum in the range  $1000 \leq N_s \leq 1500$ , where the balance between detection accuracy and communication reliability is optimal. This highlights the importance of jointly optimizing sensing and communication resources in practical integrated systems.

Finally, in Fig. 9, we analyze the impact of the quantization resolution  $\log_2 M$  on communication performance and overall estimation accuracy. As seen in Fig. 9(a), the average total variation  $\overline{\mathbb{T}\mathbb{V}}$  increases with the number of quantization bits due to the expanded message space, which makes decoding more challenging. In contrast, Fig. 9(b) shows that the GOSPA-like cost exhibits a non-monotonic trend, achieving a minimum at an intermediate quantization level around 10 bits. This reflects a fundamental tradeoff: higher resolution improves target localization but increases communication errors. Note that the performance peak at around 10 bits cannot be achieved with orthogonal codebooks. Indeed, the total

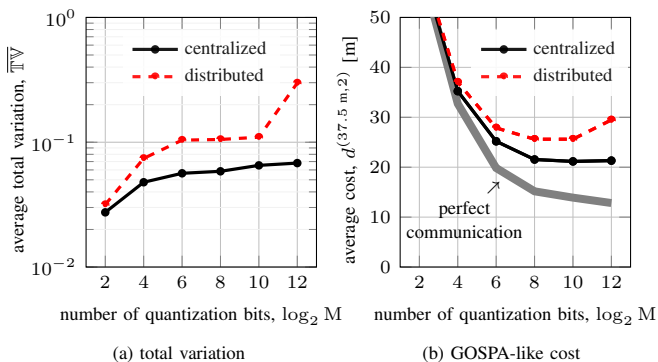


Fig. 9. Performance results vs. quantization bits  $\log_2 M$  for  $K = 200$  sensors,  $T = 50$  targets,  $\text{SNR}_{\text{rx}} = 10$  dB, and sensing blocklength  $N_s = 1000$ .

number of codewords  $\bar{M} = 9216$  far exceeds the blocklength  $N_c = 1000$ .

## VI. CONCLUSION

We have proposed TUMA for D-MIMO systems—a novel framework that allows estimation of message multiplicities under fading channels without requiring CSI at the users or the receiver. A key element of our design is location-based codebook partitioning, where users with similar large-scale fading coefficients select the same codebook. This grouping reduces path-loss variability across users. To decode the transmitted message set and their multiplicities, we developed a Bayesian decoder based on multisource approximate message passing. Centralized and distributed implementations were developed, offering a tradeoff between computational complexity (scalability) and performance in large-scale D-MIMO systems. We further demonstrated the use of TUMA in a practical application involving multi-target localization. Our framework includes a probabilistic sensing model, position quantization, and an unsourced communication layer built on the proposed TUMA scheme. We demonstrated through simulations that message collisions are highly prevalent in realistic localization scenarios, reinforcing the need for multiplicity-aware decoding. Our simulation results shed light on the fundamental tradeoffs between sensing, quantization, and communication that arise in the considered multi-target localization scenario.

The quantization resolutions in the simulations were limited to 12 bits, since the exponential growth of the message space makes AMP-based decoding computationally infeasible at higher resolutions. Larger information payloads can be accommodated using, for example, the CCS-AMP approach [33], in which larger payloads are split in small sub-blocks, each sub-block is decoded using AMP, and the sub-blocks are stitched together via an outer code. See [32] for an application of this approach to TUMA.

## APPENDIX

### A. Derivations for the Onsager Correction

For notational simplicity, as in Section III-A3, we omit the AMP iteration index ( $t$ ) and use  $\boldsymbol{\rho}_{u,1:k_u}$  and  $\mathbf{r}_u$  to denote  $\boldsymbol{\rho}_{u,m,1:k_{u,m}}$  and  $\mathbf{r}_{u,m}$ , respectively. The Onsager correction term  $\mathbf{Q}_u \in \mathbb{C}^{\text{F} \times \text{F}}$  is defined in (17) as the average Jacobian

matrix of the denoiser function  $\eta(\cdot)$ . Here, for a complex number  $r = r_x + jr_y$ , the Wirtinger derivative is defined as  $\partial(\cdot)/\partial r = (\partial(\cdot)/\partial r_x - j\partial(\cdot)/\partial r_y)/2$ . Using (11)–(15), we decompose the denoiser component  $[\eta(\mathbf{r}_u)]_b$  as

$$[\eta(\mathbf{r}_u)]_b = [\mathbf{r}_u]_b \underbrace{\sum_{k=1}^K \frac{A_b(\mathbf{r}_u, k)}{B(\mathbf{r}_u, k)}}_{F_b(\mathbf{r}_u, k)} \cdot \underbrace{\frac{C(\mathbf{r}_u, k)}{D(\mathbf{r}_u)}}_{G(\mathbf{r}_u, k)}, \quad (35)$$

$$H_b(\mathbf{r}_u)$$

where

$$A_b(\mathbf{r}_u, k) = \int_{\mathcal{D}_u^k} c_{b,u,k} p(\mathbf{r}_u | \boldsymbol{\rho}_{u,1:k}) d\boldsymbol{\rho}_{u,1:k}, \quad (36a)$$

$$c_{b,u,k} = \frac{\sqrt{\mathbb{E}_c[\sum_{i=1}^k \Sigma(\boldsymbol{\rho}_{u,i})]_{b,b}}}{[\mathbf{T}]_{b,b} + \mathbb{E}_c[\sum_{i=1}^k \Sigma(\boldsymbol{\rho}_{u,i})]_{b,b}}, \quad (36b)$$

$$B(\mathbf{r}_u, k) = \int_{\mathcal{D}_u^k} p(\mathbf{r}_u | \boldsymbol{\rho}_{u,1:k}) d\boldsymbol{\rho}_{u,1:k}, \quad (36c)$$

$$C(\mathbf{r}_u, k) = \int_{\mathcal{D}_u^k} p(\mathbf{r}_u | \boldsymbol{\rho}_{u,1:k}) p(k_u = k) d\boldsymbol{\rho}_{u,1:k}, \quad (36d)$$

$$D(\mathbf{r}_u) = \sum_{\ell=0}^K C(\mathbf{r}_u, \ell). \quad (36e)$$

Note that in (36b) we used that  $\mathbf{T}$  and  $\sum_{i=1}^k \Sigma(\boldsymbol{\rho}_{u,i})$  are both diagonal matrices. Then, the derivative of the denoiser is computed as

$$\frac{\partial[\eta(\mathbf{r}_u)]_b}{\partial[\mathbf{r}_u]_a} = \frac{\partial}{\partial[\mathbf{r}_u]_a} ([\mathbf{r}_u]_b H_b(\mathbf{r}_u)) \quad (37a)$$

$$= \delta(a - b) H_b(\mathbf{r}_u) + [\mathbf{r}_u]_b \frac{\partial H_b(\mathbf{r}_u)}{\partial[\mathbf{r}_u]_a}, \quad (37b)$$

where we note that  $H_b(\mathbf{r}_u) \in \mathbb{R}$ . Since  $H_b(\mathbf{r}_u) = \sum_{k=1}^K F_b(\mathbf{r}_u, k) \cdot G(\mathbf{r}_u, k)$ , we have

$$\frac{\partial H_b(\mathbf{r}_u)}{\partial[\mathbf{r}_u]_a} = \sum_{k=1}^K \left( G(\mathbf{r}_u, k) \frac{\partial F_b(\mathbf{r}_u, k)}{\partial[\mathbf{r}_u]_a} + F_b(\mathbf{r}_u, k) \frac{\partial G(\mathbf{r}_u, k)}{\partial[\mathbf{r}_u]_a} \right). \quad (38)$$

The derivatives of  $F_b(\mathbf{r}_u, k) = A_b(\mathbf{r}_u, k)/B(\mathbf{r}_u, k)$  and  $G(\mathbf{r}_u, k) = C(\mathbf{r}_u, k)/D(\mathbf{r}_u)$  are given by

$$\frac{\partial F_b(\mathbf{r}_u, k)}{\partial[\mathbf{r}_u]_a} = \frac{\frac{\partial A_b(\mathbf{r}_u, k)}{\partial[\mathbf{r}_u]_a} - F_b(\mathbf{r}_u, k) \frac{\partial B(\mathbf{r}_u, k)}{\partial[\mathbf{r}_u]_a}}{B(\mathbf{r}_u, k)}, \quad (39a)$$

$$\frac{\partial G(\mathbf{r}_u, k)}{\partial[\mathbf{r}_u]_a} = \frac{\frac{\partial C(\mathbf{r}_u, k)}{\partial[\mathbf{r}_u]_a} - G(\mathbf{r}_u, k) \frac{\partial D(\mathbf{r}_u)}{\partial[\mathbf{r}_u]_a}}{D(\mathbf{r}_u)}. \quad (39b)$$

The derivatives on the RHS of (39a) and (39b) can be evaluated as follows

$$\frac{\partial A_b(\mathbf{r}_u, k)}{\partial[\mathbf{r}_u]_a} = \int_{\mathcal{D}_u^k} c_{b,u,k} \frac{\partial p(\mathbf{r}_u | \boldsymbol{\rho}_{u,1:k})}{\partial[\mathbf{r}_u]_a} d\boldsymbol{\rho}_{u,1:k}, \quad (40a)$$

$$\frac{\partial B(\mathbf{r}_u, k)}{\partial[\mathbf{r}_u]_a} = \int_{\mathcal{D}_u^k} \frac{\partial p(\mathbf{r}_u | \boldsymbol{\rho}_{u,1:k})}{\partial[\mathbf{r}_u]_a} d\boldsymbol{\rho}_{u,1:k}, \quad (40b)$$

$$\frac{\partial C(\mathbf{r}_u, k)}{\partial[\mathbf{r}_u]_a} = \int_{\mathcal{D}_u^k} p(k_u = k) \frac{\partial p(\mathbf{r}_u | \boldsymbol{\rho}_{u,1:k})}{\partial[\mathbf{r}_u]_a} d\boldsymbol{\rho}_{u,1:k}, \quad (40c)$$

$$\frac{\partial D(\mathbf{r}_u)}{\partial [\mathbf{r}_u]_a} = \sum_{\ell=0}^K \int_{\mathcal{D}_u^k} p(k_u = \ell) \frac{\partial p(\mathbf{r}_u | \boldsymbol{\rho}_{u,1:\ell})}{\partial [\mathbf{r}_u]_a} d\boldsymbol{\rho}_{u,1:\ell}, \quad (40d)$$

where we have exchanged the derivative and the integral. This is justified by the Leibniz integral rule, since  $p(\mathbf{r}_u | \boldsymbol{\rho}_{u,1:k}) = \mathcal{CN}(\mathbf{r}_u; \mathbf{0}, \mathbf{T} + \mathbb{E}_c \sum_{i=1}^k \boldsymbol{\Sigma}(\boldsymbol{\rho}_{u,i}))$  is a smooth function of  $\mathbf{r}_u$  and the integration domain  $\mathcal{D}_u^k$  is fixed and bounded. The derivative of  $p(\mathbf{r}_u | \boldsymbol{\rho}_{u,1:k})$  is then

$$\begin{aligned} & \frac{\partial p(\mathbf{r}_u | \boldsymbol{\rho}_{u,1:k})}{\partial [\mathbf{r}_u]_a} \\ &= p(\mathbf{r}_u | \boldsymbol{\rho}_{u,1:k}) \frac{\partial}{\partial [\mathbf{r}_u]_a} \sum_{f=1}^F \frac{-([\mathbf{r}_u]_{f,x}^2 + [\mathbf{r}_u]_{f,y}^2)}{[\mathbf{T}]_{f,f} + \mathbb{E}_c[\sum_{i=1}^k \boldsymbol{\Sigma}(\boldsymbol{\rho}_{u,i})]_{f,f}}. \end{aligned} \quad (41)$$

To evaluate the Wirtinger derivative on the RHS of (41), note that

$$\frac{\partial \sum_{f=1}^F \frac{-([\mathbf{r}_u]_{f,x}^2 + [\mathbf{r}_u]_{f,y}^2)}{[\mathbf{T} + \mathbb{E}_c \sum_{i=1}^k \boldsymbol{\Sigma}(\boldsymbol{\rho}_{u,i})]_{f,f}}}{\partial [\mathbf{r}_u]_{a,x}} = \frac{-2[\mathbf{r}_u]_{a,x}}{[\mathbf{T} + \mathbb{E}_c \sum_{i=1}^k \boldsymbol{\Sigma}(\boldsymbol{\rho}_{u,i})]_{a,a}}, \quad (42)$$

and

$$\frac{\partial \sum_{f=1}^F \frac{-([\mathbf{r}_u]_{f,x}^2 + [\mathbf{r}_u]_{f,y}^2)}{[\mathbf{T} + \mathbb{E}_c \sum_{i=1}^k \boldsymbol{\Sigma}(\boldsymbol{\rho}_{u,i})]_{f,f}}}{\partial [\mathbf{r}_u]_{a,y}} = \frac{-2[\mathbf{r}_u]_{a,y}}{[\mathbf{T} + \mathbb{E}_c \sum_{i=1}^k \boldsymbol{\Sigma}(\boldsymbol{\rho}_{u,i})]_{a,a}}. \quad (43)$$

Hence,

$$\frac{\partial \sum_{f=1}^F \frac{-([\mathbf{r}_u]_{f,x}^2 + [\mathbf{r}_u]_{f,y}^2)}{[\mathbf{T} + \mathbb{E}_c \sum_{i=1}^k \boldsymbol{\Sigma}(\boldsymbol{\rho}_{u,i})]_{f,f}}}{\partial [\mathbf{r}_u]_a} = \frac{-[\mathbf{r}_u]_a^*}{[\mathbf{T} + \mathbb{E}_c \sum_{i=1}^k \boldsymbol{\Sigma}(\boldsymbol{\rho}_{u,i})]_{a,a}}. \quad (44)$$

Substituting (44) in (41), we have

$$\frac{\partial p(\mathbf{r}_u | \boldsymbol{\rho}_{u,1:k})}{\partial [\mathbf{r}_u]_a} = \frac{-[\mathbf{r}_u]_a^* p(\mathbf{r}_u | \boldsymbol{\rho}_{u,1:k})}{[\mathbf{T} + \mathbb{E}_c \sum_{i=1}^k \boldsymbol{\Sigma}(\boldsymbol{\rho}_{u,i})]_{a,a}}. \quad (45)$$

Substituting (45) into (40), we obtain

$$\begin{aligned} & \frac{\partial A_b(\mathbf{r}_u, k)}{\partial [\mathbf{r}_u]_a} \\ &= -[\mathbf{r}_u]_a^* \int_{\mathcal{D}_u^k} \frac{c_{b,u,k} p(\mathbf{r}_u | \boldsymbol{\rho}_{u,1:k})}{[\mathbf{T} + \mathbb{E}_c \sum_{i=1}^k \boldsymbol{\Sigma}(\boldsymbol{\rho}_{u,i})]_{a,a}} d\boldsymbol{\rho}_{u,1:k}, \end{aligned} \quad (46a)$$

$$\begin{aligned} & \frac{\partial B(\mathbf{r}_u, k)}{\partial [\mathbf{r}_u]_a} \\ &= -[\mathbf{r}_u]_a^* \int_{\mathcal{D}_u^k} \frac{p(\mathbf{r}_u | \boldsymbol{\rho}_{u,1:k})}{[\mathbf{T} + \mathbb{E}_c \sum_{i=1}^k \boldsymbol{\Sigma}(\boldsymbol{\rho}_{u,i})]_{a,a}} d\boldsymbol{\rho}_{u,1:k}, \end{aligned} \quad (46b)$$

$$\begin{aligned} & \frac{\partial C(\mathbf{r}_u, k)}{\partial [\mathbf{r}_u]_a} \\ &= -[\mathbf{r}_u]_a^* \int_{\mathcal{D}_u^k} \frac{p(k_u = k) p(\mathbf{r}_u | \boldsymbol{\rho}_{u,1:k})}{[\mathbf{T} + \mathbb{E}_c \sum_{i=1}^k \boldsymbol{\Sigma}(\boldsymbol{\rho}_{u,i})]_{a,a}} d\boldsymbol{\rho}_{u,1:k}, \end{aligned} \quad (46c)$$

$$\begin{aligned} & \frac{\partial D(\mathbf{r}_u)}{\partial [\mathbf{r}_u]_a} \\ &= -[\mathbf{r}_u]_a^* \sum_{\ell=0}^K \int_{\mathcal{D}_u^\ell} \frac{p(k_u = \ell) p(\mathbf{r}_u | \boldsymbol{\rho}_{u,1:\ell})}{[\mathbf{T} + \mathbb{E}_c \sum_{i=1}^k \boldsymbol{\Sigma}(\boldsymbol{\rho}_{u,i})]_{a,a}} d\boldsymbol{\rho}_{u,1:\ell}. \end{aligned} \quad (46d)$$

We obtain the desired result by combining (37)–(39) and (46).

## B. Distributed Multisource AMP

In the distributed AMP setup, each AP  $b$  processes its local effective received signal  $\mathbf{r}_{b,u,m} \in \mathbb{C}^A$  for each codeword  $\mathbf{c}_{u,m}$ . The local likelihood  $p_b(\mathbf{r}_{b,u,m} | \boldsymbol{\rho}_{u,1:k})$  is given by

$$p_b(\mathbf{r}_{b,u,m} | \boldsymbol{\rho}_{u,1:k}) = \mathcal{CN}(\mathbf{r}_{b,u,m}; \mathbf{0}, \text{Cov}_b), \quad (47)$$

where  $\text{Cov}_b = \mathbf{T}_b + \mathbb{E}_c \sum_{i=1}^k \boldsymbol{\Sigma}_b(\boldsymbol{\rho}_{u,i})$  is the local  $A \times A$  covariance matrix. Here,  $\mathbf{T}_b$  is the covariance matrix of the local residual noise computed at AP  $b$  and  $\boldsymbol{\Sigma}_b(\boldsymbol{\rho}) = \gamma_b(\boldsymbol{\rho}) \mathbf{I}_A$  is the LSFC between the user in position  $\boldsymbol{\rho}$  and AP  $b$ . Let  $\text{Cov} = \mathbf{T} + \mathbb{E}_c \sum_{i=1}^k \boldsymbol{\Sigma}(\boldsymbol{\rho}_{u,i})$  denote the global  $F \times F$  covariance matrix. The key observation is that, since both  $\boldsymbol{\Sigma}(\boldsymbol{\rho}_{u,i})$  and  $\mathbf{T}$  have a block diagonal structure, with the  $\{\boldsymbol{\Sigma}_b(\boldsymbol{\rho}_{u,i})\}$  and the  $\{\mathbf{T}_b\}$  as blocks, then

$$p(\mathbf{r}_{u,m} | \boldsymbol{\rho}_{u,1:k}) = \prod_{b=1}^B p_b(\mathbf{r}_{b,u,m} | \boldsymbol{\rho}_{u,1:k}). \quad (48)$$

The Onsager correction term in distributed AMP is computed locally at each AP  $b$  as  $[\mathbf{Q}_{u,b}]_{a,c} = (1/M) \sum_{m=1}^M \partial[\eta_u(\mathbf{r}_{b,u,m})]_c / \partial [\mathbf{r}_{b,u,m}]_a$ , and aggregated at the CPU as  $[\mathbf{Q}_u]_{a,c} = \sum_{b=1}^B [\mathbf{Q}_{u,b}]_{a,c}$ .

## REFERENCES

- [1] K.-H. Ngo, D. P. Krishnan, K. Okumus, G. Durisi, and E. G. Ström, "Type-based unsourced multiple access," in *Proc. IEEE Workshop Signal Process. Adv. Wireless Commun. (SPAWC)*, Lucca, Italy, Sep. 2024, pp. 911–915.
- [2] K. Okumus, K.-H. Ngo, G. Durisi, and E. G. Ström, "Type-based unsourced multiple access over fading channels with cell-free massive MIMO," in *Proc. IEEE Int. Symp. Inf. Theory (ISIT)*, Ann Arbor, MI, USA, June 2025.
- [3] X. Chen, D. W. K. Ng, W. Yu, E. G. Larsson, N. Al-Dhahir, and R. Schober, "Massive access for 5G and beyond," *IEEE J. Sel. Areas Commun.*, vol. 39, no. 3, pp. 615–637, Mar. 2021.
- [4] Y. Wu, X. Gao, S. Zhou, W. Yang, Y. Polyanskiy, and G. Caire, "Massive access for future wireless communication systems," *IEEE Wireless Commun.*, vol. 27, no. 4, pp. 148–156, Aug. 2020.
- [5] A. E. Kalor, G. Durisi, S. Coleri, S. Parkvall, W. Yu, A. Mueller, and P. Popovski, "Wireless 6G connectivity for massive number of devices and critical services," *Proc. IEEE*, Nov. 2024.
- [6] Y. Polyanskiy, "A perspective on massive random-access," in *Proc. IEEE Int. Symp. Inf. Theory (ISIT)*, Aachen, Germany, June 2017, pp. 2523–2527.
- [7] A. Lanchio, A. Fengler, and Y. Polyanskiy, "Finite-blocklength results for the A-channel: Applications to unsourced random access and group testing," in *Proc. Allerton Conf. Communication, Control and Computing*, Monticello, IL, USA, Sep. 2022.
- [8] J. Gao, Y. Wu, S. Shao, W. Yang, and H. V. Poor, "Energy efficiency of massive random access in MIMO quasi-static rayleigh fading channels with finite blocklength," *IEEE Trans. Inf. Theory*, vol. 69, no. 3, pp. 1618–1657, Mar. 2023.
- [9] K. Andreev, D. Ustinova, and A. Frolov, "Unsourced random access with the MIMO receiver: Projection decoding analysis," *IEEE Wireless Commun. Lett.*, vol. 13, no. 1, pp. 69–73, Jan. 2024.
- [10] K.-H. Ngo, A. Lanchio, G. Durisi, and A. Graell i Amat, "Unsourced multiple access with random user activity," *IEEE Trans. Inf. Theory*, vol. 69, no. 7, pp. 4537–4558, July 2023.
- [11] K. Andreev, P. Rybin, and A. Frolov, "Unsourced random access," *Foundations and Trends® in Communications and Information Theory*, vol. 22, no. 5-6, pp. 605–842, Aug. 2025.
- [12] A. Fengler, P. Jung, and G. Caire, "SPARCs for unsourced random access," *IEEE Trans. Inf. Theory*, vol. 67, no. 10, pp. 6894–6915, Oct. 2021.

- [13] V. K. Amalladinne, A. K. Pradhan, C. Rush, J.-F. Chamberland, and K. R. Narayanan, "Unsourced random access with coded compressed sensing: Integrating AMP and belief propagation," *IEEE Trans. Inf. Theory*, vol. 68, no. 4, pp. 2384–2409, Apr. 2022.
- [14] A. Pradhan, V. Amalladinne, A. Vem, K. R. Narayanan, and J.-F. Chamberland, "A joint graph based coding scheme for the unsourced random access Gaussian channel," in *Proc. IEEE Global Commun. Conf. (GLOBECOM)*, Waikoloa, HI, USA, Dec. 2019.
- [15] A. Vem, K. R. Narayanan, J.-F. Chamberland, and J. Cheng, "A user-independent successive interference cancellation based coding scheme for the unsourced random access Gaussian channel," *IEEE Trans. Commun.*, vol. 67, no. 12, pp. 8258–8272, Dec. 2019.
- [16] A. Fengler, S. Haghghatshoar, P. Jung, and G. Caire, "Non-Bayesian activity detection, large-scale fading coefficient estimation, and unsourced random access with a massive MIMO receiver," *IEEE Trans. Inf. Theory*, vol. 67, no. 5, pp. 2925–2951, May 2021.
- [17] Z. Han, X. Yuan, C. Xu, S. Jiang, and X. Wang, "Sparse Kronecker-product coding for unsourced multiple access," *IEEE Wireless Commun. Lett.*, vol. 10, no. 10, pp. 2274–2278, Oct. 2021.
- [18] A. Decurninge, I. Land, and M. Guillaud, "Tensor-based modulation for unsourced massive random access," *IEEE Wireless Commun. Lett.*, vol. 10, no. 3, pp. 552–556, Mar. 2021.
- [19] A. K. Pradhan, V. K. Amalladinne, K. R. Narayanan, and J.-F. Chamberland, "Polar coding and random spreading for unsourced multiple access," in *Proc. IEEE Int. Conf. Commun. (ICC)*, Dublin, Ireland, June 2020.
- [20] J. Hoffman and R. Mahler, "Multitarget miss distance via optimal assignment," *IEEE Trans. Syst. Man. Cybern. A Syst. Human.*, vol. 34, no. 3, pp. 327–336, May 2004.
- [21] D. Schuhmacher, B.-T. Vo, and B.-N. Vo, "A consistent metric for performance evaluation of multi-object filters," *IEEE Trans. Signal Process.*, vol. 56, no. 8, pp. 3447–3457, Aug. 2008.
- [22] A. S. Rahmattullah, A. F. García-Fernández, and L. Svensson, "Generalized optimal sub-pattern assignment metric," in *Proc. Int. Conf. Inf. Fus. (FUSION)*, Xi'an, China, July 2017, pp. 182–189.
- [23] L. Qiao, Z. Gao, M. Boloursaz Mashhadi, and D. Gündüz, "Massive digital over-the-air computation for communication-efficient federated edge learning," *IEEE J. Sel. Areas Commun.*, vol. 42, no. 11, pp. 3078–3094, Nov. 2024.
- [24] K. Okumus, K.-H. Ngo, U. K. Ganesan, G. Durisi, E. G. Ström, and S. R. Pandey, "Type-based unsourced federated learning with client self-selection," Feb. 2026. [Online]. Available: <https://arxiv.org/abs/2602.06601>
- [25] C. Bian, Y. Shao, and D. Gündüz, "Wireless point cloud transmission," in *Proc. IEEE Workshop Signal Process. Adv. Wireless Commun. (SPAWC)*, Lucca, Italy, Sep. 2024, pp. 851–855.
- [26] K. Liu and A. Sayeed, "Asymptotically optimal decentralized type-based detection in wireless sensor networks," in *Proc. IEEE Int. Conf. Acoustics, Speech, and Signal Processing (ICASSP)*, vol. 3, Montreal, QC, Canada, May 2004, pp. iii–873.
- [27] G. Mergen and L. Tong, "Type based estimation over multiaccess channels," *IEEE Trans. Signal Process.*, vol. 54, no. 2, pp. 613–626, Feb. 2006.
- [28] J. Dommel, Z. Utkovski, S. Stańczak, and O. Simeone, "Joint source-channel coding and Bayesian message passing detection for grant-free radio access in IoT," in *Proc. IEEE Int. Conf. Acoustics, Speech, and Signal Processing (ICASSP)*, Barcelona, Spain, May 2020, pp. 8574–8578.
- [29] J. Dommel, Z. Utkovski, O. Simeone, and S. Stańczak, "Joint source-channel coding for semantics-aware grant-free radio access in IoT fog networks," *IEEE Signal Process. Lett.*, vol. 28, pp. 728–732, Apr. 2021.
- [30] M. Zhu, C. Feng, C. Guo, N. Jiang, and O. Simeone, "Information bottleneck-inspired type based multiple access for remote estimation in IoT systems," *IEEE Signal Process. Lett.*, vol. 30, pp. 403–407, Apr. 2023.
- [31] X. Meng, L. Zhang, C. Wang, L. Wang, Y. Wu, Y. Chen, and W. Wang, "Advanced NOMA receivers from a unified variational inference perspective," *IEEE J. Select. Areas Commun.*, vol. 39, no. 4, pp. 934–948, Apr. 2021.
- [32] D. P. Krishnan, K. Okumus, K.-H. Ngo, and G. Durisi, "An achievability bound for type-based unsourced multiple access," in *Proc. IEEE Int. Symp. Inf. Theory (ISIT)*, Ann Arbor, MI, USA, June 2025.
- [33] V. K. Amalladinne, J.-F. Chamberland, and K. R. Narayanan, "A coded compressed sensing scheme for unsourced multiple access," *IEEE Trans. Inf. Theory*, vol. 66, no. 10, pp. 6509–6533, Oct. 2020.
- [34] E. Gkiouzepe, B. Çakmak, M. Opper, and G. Caire, "Joint message detection, channel, and user position estimation for unsourced random access in cell-free networks," in *Proc. IEEE Workshop Signal Process. Adv. Wireless Commun. (SPAWC)*, Lucca, Italy, Sep. 2024, pp. 151–155.
- [35] B. Çakmak, E. Gkiouzepe, M. Opper, and G. Caire, "Joint message detection and channel estimation for unsourced random access in cell-free user-centric wireless networks," *IEEE Trans. Inf. Theory*, vol. 71, no. 5, pp. 3614–3643, May 2025.
- [36] B. Çakmak and G. Caire, "Multi-source approximate message passing with random semi-unitary dictionaries," in *Proc. IEEE Int. Symp. Inf. Theory (ISIT)*, June 2025.
- [37] J. Bai and E. G. Larsson, "Activity detection in distributed MIMO: Distributed AMP via likelihood ratio fusion," *IEEE Wireless Commun. Lett.*, vol. 11, no. 10, pp. 2200–2204, Oct. 2022.
- [38] H. Wymeersch and G. Seco-Granados, "Adaptive detection probability for mmWave 5G SLAM," in *Proc. 6G Wireless Summit (6G SUMMIT)*, Levi, Finland, Mar. 2020.
- [39] M. Bayati and A. Montanari, "The dynamics of message passing on dense graphs, with applications to compressed sensing," *IEEE Trans. Inf. Theory*, vol. 57, no. 2, p. 764–785, Feb. 2011.
- [40] P. Billingsley, *Probability and Measure*, Anniversary ed. New York, NY, USA: John Wiley & Sons, Inc., Jan. 2012.
- [41] S. M. Kay, *Fundamentals of statistical signal processing: estimation theory*. Upper Saddle River, NJ, USA: Prentice-Hall, Inc., Mar. 1993.
- [42] Ö. T. Demir, E. Björnson, and L. Sanguinetti, "Foundations of user-centric cell-free massive MIMO," *Foundations and Trends® in Signal Processing*, vol. 14, no. 3-4, pp. 162–472, Jan. 2021.
- [43] A. Shahmansoori, G. E. Garcia, G. Destino, G. Seco-Granados, and H. Wymeersch, "Position and orientation estimation through millimeter-wave mimo in 5G systems," *IEEE Trans. Wireless Commun.*, vol. 17, no. 3, pp. 1822–1835, Mar. 2018.
- [44] Z. Abu-Shaban, X. Zhou, T. Abhayapala, G. Seco-Granados, and H. Wymeersch, "Error bounds for uplink and downlink 3D localization in 5G millimeter wave systems," *IEEE Trans. Wireless Commun.*, vol. 17, no. 8, pp. 4939–4954, Aug. 2018.
- [45] Y. Ge, O. Kallio, H. Kim, J. Talvitie, S. Kim, L. Svensson, M. Valkama, and H. Wymeersch, *MmWave Mapping and SLAM for 5G and Beyond*. Singapore: Springer Nature, July 2023, pp. 445–475.
- [46] G. Peyré and M. Cuturi, "Computational optimal transport: With applications to data science," *Foundations and Trends® in Machine Learning*, vol. 11, no. 5-6, pp. 355–607, Feb. 2019.
- [47] J. A. Zhang, M. L. Rahman, K. Wu, X. Huang, Y. J. Guo, S. Chen, and J. Yuan, "Enabling joint communication and radar sensing in mobile networks—a survey," *IEEE Commun. Surv. & Tut.*, vol. 24, no. 1, pp. 306–345, Oct. 2022.
- [48] F. Liu, C. Masouros, A. P. Petropulu, H. Griffiths, and L. Hanzo, "Joint radar and communication design: Applications, state-of-the-art, and the road ahead," *IEEE Trans. Commun.*, vol. 68, no. 6, pp. 3834–3862, Feb. 2020.
- [49] F. Liu, Y. Cui, C. Masouros, J. Xu, T. X. Han, Y. C. Eldar, and S. Buzzi, "Integrated sensing and communications: Toward dual-functional wireless networks for 6G and beyond," *IEEE J. Sel. Areas Commun.*, vol. 40, no. 6, pp. 1728–1767, Mar. 2022.